remote sensing

MDPI

Article

Comparison of Time-Lapse Ground-Penetrating Radar and Electrical Resistivity Tomography Surveys for Detecting Pig (*Sus* spp.) Cadaver Graves in an Australian Environment

Victoria Berezowski [1,2,*], Xanthé Mallett [1], Dilan Seckiner [3], Isabella Crebert [1], Justin Ellis [1], Gabriel C. Rau [4] and Ian Moffat [5]

[1] School of Law and Justice, College of Human and Social Futures, University of Newcastle, Newcastle, NSW 2300, Australia
[2] School of Life and Environmental Sciences, Faculty of Science, Engineering and Built Environment, Deakin University, Waurn Ponds, VIC 3216, Australia
[3] School of Biomedical Sciences, Faculty of Medicine and Health, University of New South Wales, Sydney, NSW 2052, Australia
[4] School of Environmental and Life Sciences, College of Engineering, Science, and Environment, University of Newcastle, Newcastle, NSW 2308, Australia
[5] Archaeology, College of Humanities, Arts and Social Sciences, Flinders University, Adelaide, SA 5001, Australia
* Correspondence: tori.b@deakin.edu.au

check for updates

Citation: Berezowski, V.; Mallett, X.; Seckiner, D.; Crebert, I.; Ellis, J.; Rau, G.C.; Moffat, I. Comparison of Time-Lapse Ground-Penetrating Radar and Electrical Resistivity Tomography Surveys for Detecting Pig (*Sus* spp.) Cadaver Graves in an Australian Environment. *Remote Sens.* **2024**, *16*, 3498. https://doi.org/10.3390/rs16183498

Academic Editor: David Gomez-Ortiz

Received: 25 July 2024
Revised: 27 August 2024
Accepted: 19 September 2024
Published: 20 September 2024

Correction Statement: This article has been republished with a minor change. The change does not affect the scientific content of the article and further details are available within the backmatter of the website version of this article.

Abstract: Locating clandestine graves presents significant challenges to law enforcement agencies, necessitating the testing of grave detection techniques. This experimental study, conducted under Australian field conditions, assesses the effectiveness of time-lapse ground-penetrating radar (GPR) and electrical resistivity tomography (ERT) in detecting pig burials as simulated forensic cases. The research addresses two key questions: (1) observability of graves using GPR and ERT, and (2) changes in geophysical responses with reference to changing climatic conditions. The principal novelty of this research is its Australian focus—this is the first time-lapse GPR and ERT study used to locate clandestine graves in Australia. The results reveal that both GPR and ERT can detect graves; however, ERT demonstrates greater suitability in homogeneous soil and anomalously wet climate conditions, with the detectability affected by grave depth. This project also found that resistivity values are likely influenced by soil moisture and decomposition fluids; however, these parameters were not directly measured in this study. Contrastingly, although GPR successfully achieved 2 m penetration in each survey, the site's undeveloped soil likely resulted in inconsistent detectability. The findings underscore the significance of site-specific factors when employing GPR and/or ERT for grave detection, including soil homogeneity, climate conditions, water percolation, and body decomposition state. These findings offer practical insights into each technique's utility as a search tool for missing persons, aiding law enforcement agencies with homicide cases involving covert graves.

Keywords: forensic geophysics; ground-penetrating radar; electrical resistivity tomography; clandestine grave; missing person; homicide

1. Introduction

After a homicide takes place, offenders may choose to engage in detection avoidance behaviours [1,2], such as burying their victims in a clandestine or covert grave (defined as an illegal burial containing human remains [3]—used interchangeably in this project). Often, these types of graves are only found by chance [1] or with specific case information (provided by a witness or person of interest, for example), making finding their location a key challenge to law enforcement agencies. With the high number of missing persons, especially in Australia (currently 2600 individuals missing for three months or more [4]), the importance of being able to locate clandestine graves cannot be overstated. The location of

covert graves can result in the successful prosecution of those responsible for a crime [5,6], as well as providing answers to the family about their loved one's death.

There are many grave location techniques available, ranging from a pedestrian survey to remote sensing [7]—an in-depth review of clandestine grave search methods can be found in the study by Donnelly and Harrison [8]. The choice of search technique depends on time and monetary constraints, as well as equipment, and consultant availability. One approach that is underutilised in forensic investigations is the use of geophysical techniques. Although geophysical techniques, such as ground-penetrating radar (GPR) and resistivity methods (electrical resistivity tomography [ERT] and fixed-point resistivity [FPR]), are commonly used for grave detection in archaeological contexts, their use in investigative communities has not reached the same level of acceptance.

Geophysical techniques can measure properties in the subsurface in a non-invasive and non-destructive manner. When applied to grave detection, a geophysical survey will utilise a technique that can measure a physical property (i.e., electrical conductivity and resistivity, gravity, magnetic susceptibility, and acoustic velocity [9]) that is impacted by the target of the investigation [10,11], including the disturbed soil, a decomposing body [12,13], associated items, such as body wrapping (i.e., tarpaulin) [14], clothing, personal items, or weapons [12,13], and very rarely, skeletal remains [15]. GPR is the most commonly used geophysical technique for grave location due to its rapid data collection capabilities and high resolution [11]; however, ERT may also be useful because it can achieve better depth penetration.

The aim of this experimental study is to assess the changes in the geophysical responses of graves, via a time-lapse study, under Australian field conditions, to evaluate each technique's utility as a search tool. More specifically, this research will document and analyse the changes in the GPR and ERT responses of buried domestic pig (*Sus* spp.) cadavers, to simulate human burials, over a period of twenty months at a research site in Western Sydney. Three graves, composed of two single burials containing one pig each and one mass grave containing three pigs, were created in March 2021 and systematically monitored until November 2022. Identically conducted GPR and ERT surveys were undertaken prior and directly after the pig graves were created (to act as a control for the post-burial surveys), and this process was repeated at one, eight, fourteen, and twenty months post-burial. The results of these surveys were interpreted with reference to measurements of rainfall and temperature from a local weather station and measurement of sediment properties from the excavations. The final interpretations were shaped by two key variables: (1) observability of graves using GPR and ERT, and (2) changes in geophysical responses with reference to changing climatic conditions.

Similar experimental studies have been conducted around the world, including in Australia [16], the USA [12,13], the UK [17–19], and South America [20,21], using varied survey parameters. Powell [16] found that a 200 MHz antennae GPR found anomalies consistent with the location of eight-month-old naked pig graves, in calcareous soil, in a hot and dry environment. Pringle and colleagues [17–19] monitored naked (amongst other types of burials not relevant to this project) pig burials with a 110, 225, 450, and 900 MHz antennae GPR and a 0.5 m electrode spacing ERT for a period of 10 years. The results showed that the GPR (at all frequencies) could detect the graves as a low-amplitude hyperbolic reflection for up to six years, and the ERT observed the graves as a low-resistivity anomaly for up to four years. Molina and colleagues [20] conducted geophysical surveys, using GPR, magnetic susceptibility, bulk ground conductivity, and ERT, of pig cadaver graves (as well as other types of burials not relevant to this research) with a depth of 1.2 m over a period of 22 months post-burial. The researchers found that the pig burials, which were half-clothed, were optimally imaged with a 250 MHz antennae GPR. Finally, Cavalcanti et al. [21] monitored naked pig burials (amongst other types not relevant to this project) with a 400 MHz antenna GPR 15 days after burial and with a 0.5 m and 1.0 m electrode spacing ERT set up six-months after burial. The results showed that the pigs attenuated the GPR signal and that the ERT poorly imaged the naked pig burials.

The principal novelty of this study is its Australian focus—it is the first time-lapse GPR and ERT study conducted to locate clandestine graves in Australia. While some similar work was undertaken in South Australia by Powell [16], the study site had very different soil and climate conditions, and time-lapse surveys were not undertaken. This research offers additional new insight into the GPR and ERT responses of naked pig burials, including a range of grave depths, a higher-resolution electrode spacing, and the inclusion of a mass grave. Firstly, the depth of the graves in most experimental studies ranged between 0.5 m and 1.2 m, with most averaging at 0.8 m; however, this project includes a grave that is 1.8 m deep. This will allow for a better understanding of how depth affects the geophysical responses. Secondly, the electrode spacing for the current project is 0.25 m, which will achieve a higher resolution while still penetrating the depth of the deepest grave. Finally, this project includes a mass grave (defined here as a grave with more than one individual), which is not commonly encountered in the literature. Doro et al. [22,23] include mass graves in their experimental study; however, they use human cadavers in the graves instead of pigs.

2. Materials and Methods

2.1. Study Site

A plot of land measuring 20 m × 10 m was provided by the Australian Facility for Taphonomic Experimental Research (AFTER) for this study. The study site is in Western Sydney (Australia—Figure 1B), located 19 m above sea level in a Cumberland dry sclerophyll forest. This location is underlain by Hawkesbury sandstone with minor shale lenses [24], and the soil is a poorly developed sandy Tenosol [25]. During the study period (March 2021 to November 2022), the site experienced temperatures ranging from 2–36.1 °C with an average temperature of 16.6 °C and had rainfall ranging from 2.4 to 591.2 mm with the total and average rainfall being 2526 mm and 113.8 mm, respectively. Due to a La Niña phase of the El Niño Southern Oscillation (ENSO), NSW experienced higher-than-usual amounts of rainfall and increased percentages of soil moisture over the study period, with the highest annual total rainfall in at least 20 years for the region. The temperature, rainfall (i.e., precipitation), and soil moisture data were sourced from the Bureau of Meteorology (Richmond RAAF weather station [ID 067105], located approximately 12 km NE of the site) and are provided in Figure 2.

2.2. Set Up, Simulated Grave Creation, and Survey Repetitions

The geophysical survey line was placed down the middle of the study site, approximately perpendicular in orientation to the pig cadavers. Considering that the total length of an ERT line dictates the depth penetration (i.e., depth is approx. 20% of length), and that there is an inverse relationship between electrode spacing and the resulting resolution (i.e., increased spacing results in decreased resolution [3,11,14,26]), a 0.25 m electrode spacing was chosen, which resulted in a 16 m survey line (~16 m GPR line and 15.75 m ERT line with 64 ERT electrodes), oriented NE–SW and sloping slightly to the NE. Although both 0.5 m and 0.25 m electrode spacing can be used to detect forensically significant graves, Doro et al. [23] found that the 0.25 m electrode spacing improved resolution and was thus chosen for this research project. To ensure consistency across each of the geophysical surveys, and to allow for meaningful comparisons, the start and end pegs were kept in the ground for the duration of the study period. The exact placement of the survey line, as well as the placement of the graves along the line were mapped using a Leica TS09 total station, which was georectified using a CHC X90-Opus static GPS and postprocessed using the Auspos service. This was augmented by pre- and post-burial surveys of the site undertaken with a DJI Mavic Air drone, the results of which were postprocessed to create 3D point clouds and orthophotos using Agisoft Metashape Professional.

Although it is standard practice in forensic investigations to collect geophysical data using a grid, this study specifically chose to use only a single GPR and ERT line to examine how

the geophysical responses of known subsurface features changed with time. Additionally, this approach minimised the time required to undertake the fieldwork for this project.

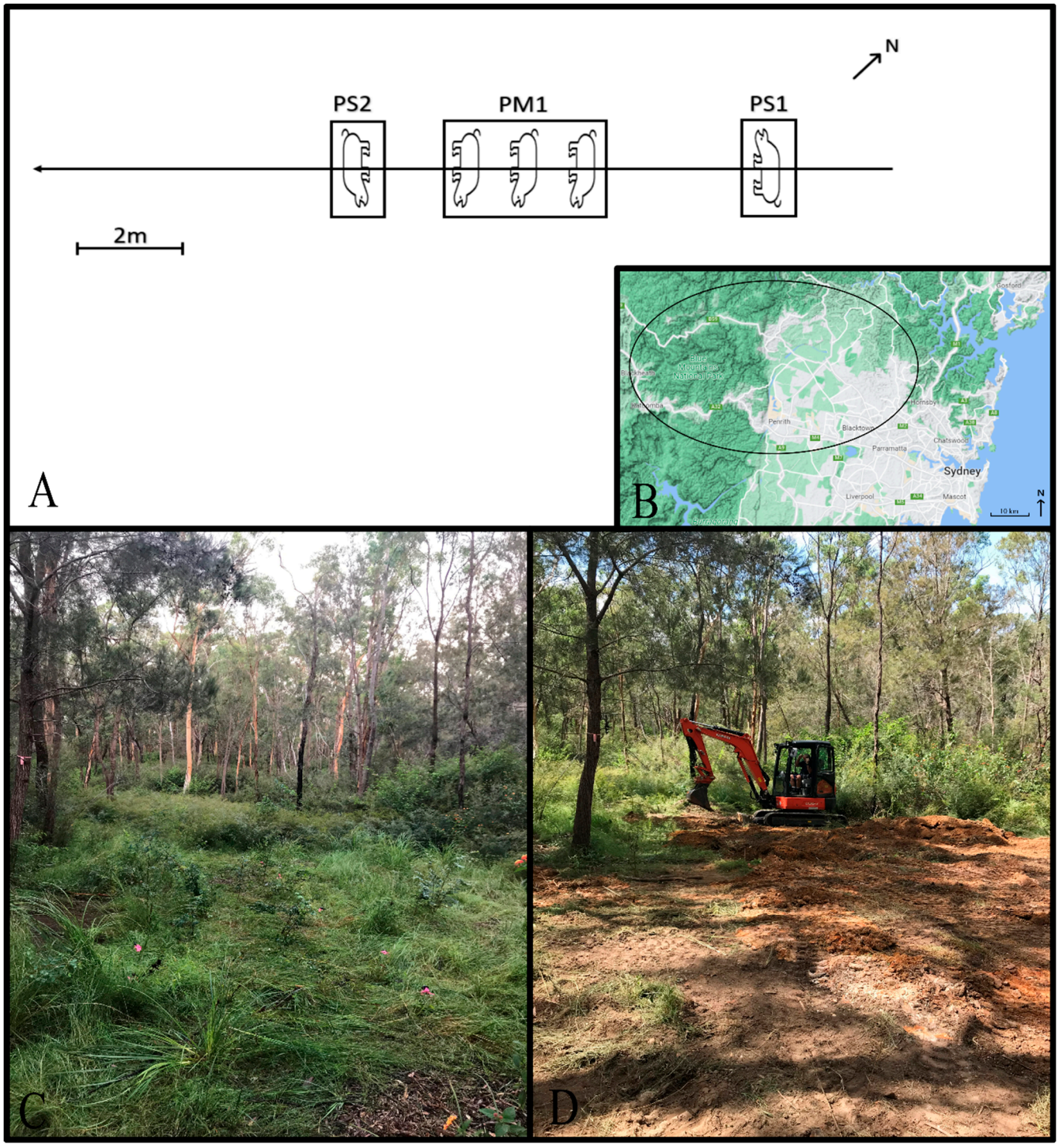

Figure 1. Grave schematic, site map, and site conditions. (**A**) Grave set up: The graves were dug in a NW/SE orientation along a 16 m survey line. The arrow denotes the direction of the survey line, and the pig icons signify the direction the pigs were placed in each grave. (**B**) The general area of the AFTER animal site (due to confidentiality, the exact location of the site cannot be included). The satellite map was sourced from Google Maps©. (**C**) The study site before grave creation, highlighting the abundance of native plant life before being mechanically cleared. (**D**) The study site after grave creation, highlighting the highly disturbed nature of the surface soil.

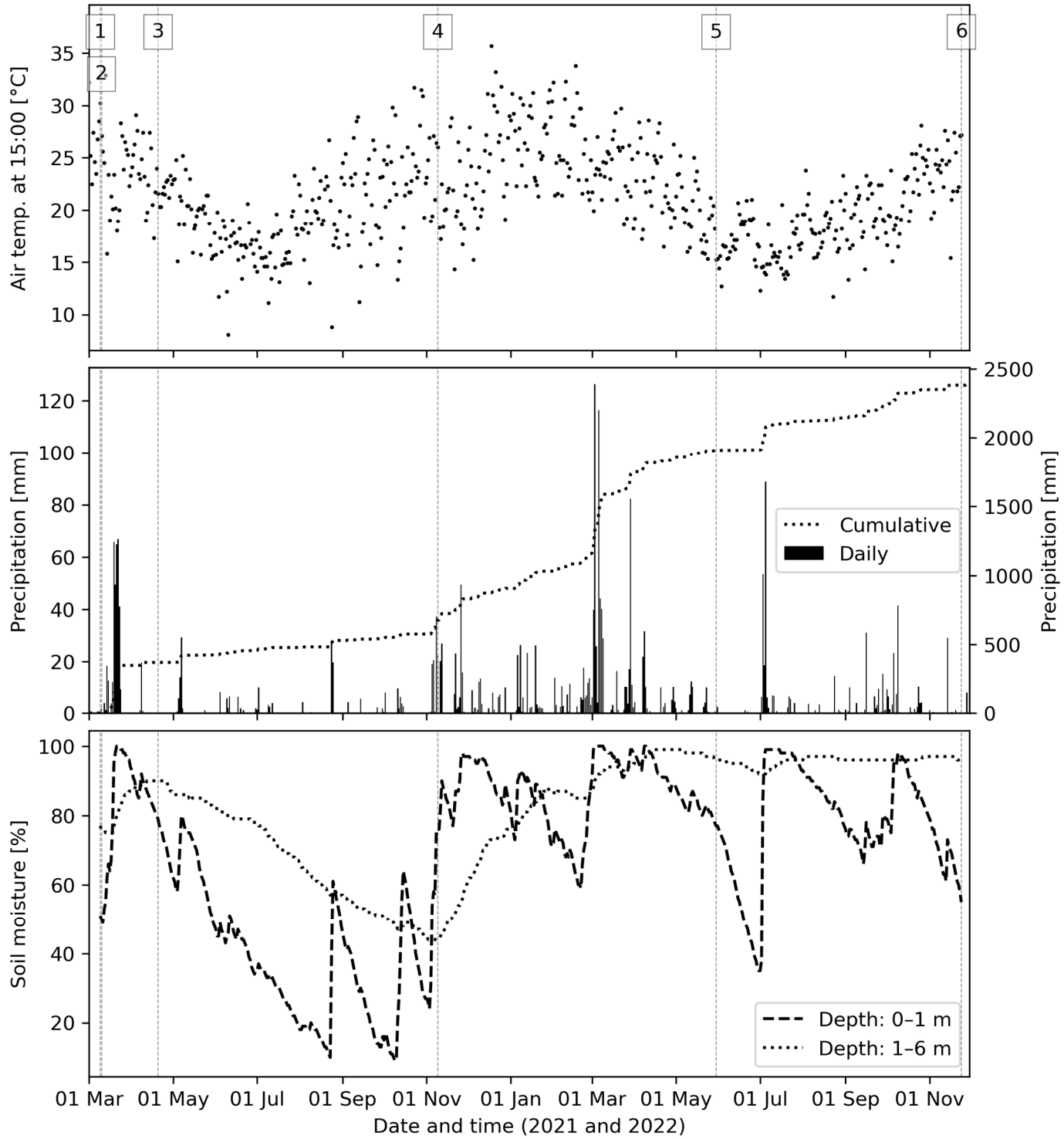

Figure 2. Temperature and soil moisture data. Vertical dotted lines with numbers 1–6 denote the survey dates. **TOP**: Monthly mean temperatures from March 2021 to November 2022. Mean temperatures were calculated using the daily 3 p.m. temperatures throughout the survey period. Note that there is only one line for March 2021; however, there were two survey days (pre-burial on 9 March and post-burial on 10 March). **MIDDLE**: Daily (black bars) and cumulative (dotted line) rainfall from March 2021 to November 2022. **BOTTOM**: Shallow (0–1 m deep; thick line) and deep (1–6 m; thin line) soil moisture data from March 2021 to November 2022. For each image, the vertical dotted lines and numbers denote the survey date. Data sourced from The Bureau of Meteorology, Richmond RAAF weather station (ID# 067105).

On the morning of 9 March 2021, the pre-burial GPR and ERT surveys were conducted using the methods outlined below on the undisturbed study site (Figure 1C). The site was subsequently cleared, and three simulated graves, including two single graves and one mass grave, were dug with a Kubota U35-4 excavator (see Table 1 for grave details). The single graves, referred to as PS1 (pig single 1) and PS2 (pig single 2), were both 2 m long, 1 m wide, and 0.5 m and 1.8 m deep, respectively. The mass grave, referred to as PM1 (pig mass 1), was 2 m long, 2.5 m wide, and 1 m deep (shown in Figure 1A). The lengths and widths of each grave were dictated by the average size of an adult human; however, the depths were chosen to mirror real-life scenarios. More specifically, PS1 and PM1 were dug 0.50 m and 1 m deep, respectively, as the literature states that most forensic burials are within this range [17,27]. Although PS2 is deeper than most forensic burials (most forensic burials are not deeper than 1 m; however, there are cases involving deeper graves. For example, in 2018, South Australian Police excavated the potential grave of the missing Beaumont siblings that was found to be 2 m deep (see Berezowski et al. [28])), it allows for an analysis of how depth affects the geophysical responses and provides an analogue to cemetery burials. Both single and mass graves were included so that the results could be used to help law enforcement with cases of both single and multiple homicides (where the victim(s) is found in a clandestine grave), as well as human rights investigations that involve locating mass graves.

Table 1. Summary of the burial types, the sex and weight of each pig cadaver, and their placement within each grave.

Grave ID	Grave Dimensions (LxWxD in m)	Type (and # of Pig Cadavers)	Sex	Weight (kg)	Position in Grave
PS1	2 × 1 × 0.5	Single (1)	Female	60	Side laying; head at NW end of grave and facing SW
PM1	2 × 2.5 × 1	Mass (3)	Males	70, 80, 90	Side laying; head at SE end of grave and facing SW
PS2	2 × 1 × 1.8	Single (1)	Female	50	Side laying; head at SE end of grave and facing NE

After the graves were dug, five pig cadavers were placed in the graves. The soil was replaced over each of the cadavers (see Figure 1D) and the post-burial GPR and ERT surveys were conducted. In total, the study site was surveyed six times over a twenty-month period, including pre-burial and directly post-burial, and then one, eight, fourteen, and twenty months post-burial.

Due to limited access to human donors, this research had to rely solely on pig cadavers; however, Berezowski et al. [29] found that pigs are adequate human proxies for the geophysical detection of covert graves. The use of animal cadavers for this research project was approved by the Animal Care and Ethics Committee from the University of Newcastle, and the research was conducted in accordance with all applicable national and international guidelines. As per the ethical guidelines provided by AFTER and The University of Newcastle, the pigs were killed with a captive head bolt, delivered to the site, and placed in the graves on the same day.

2.3. GPR Surveys

A Mala X3M 500 MHz GPR system (shown in Figure 3A) was used, with survey parameters that include 4 stacks, 56.3 ns time, 1024 samples, and a 2 cm trace increment. The pre-burial and post-burial GPR lines were collected using a 10 cm trace increment, due to a faulty measurement wheel. Once the data were collected, a series of processing steps were undertaken in ReflexW including, (1) moving the start time via a static correction, (2) subtracting mean from traces via a 'de-wow', (3) applying an energy decay gain, (4) applying a bandpass Butterworth filter, (5) applying a 2D running average filter, and

(6) applying a time cut to 50 ns. The resulting profiles were then exported and compiled in InkScape.

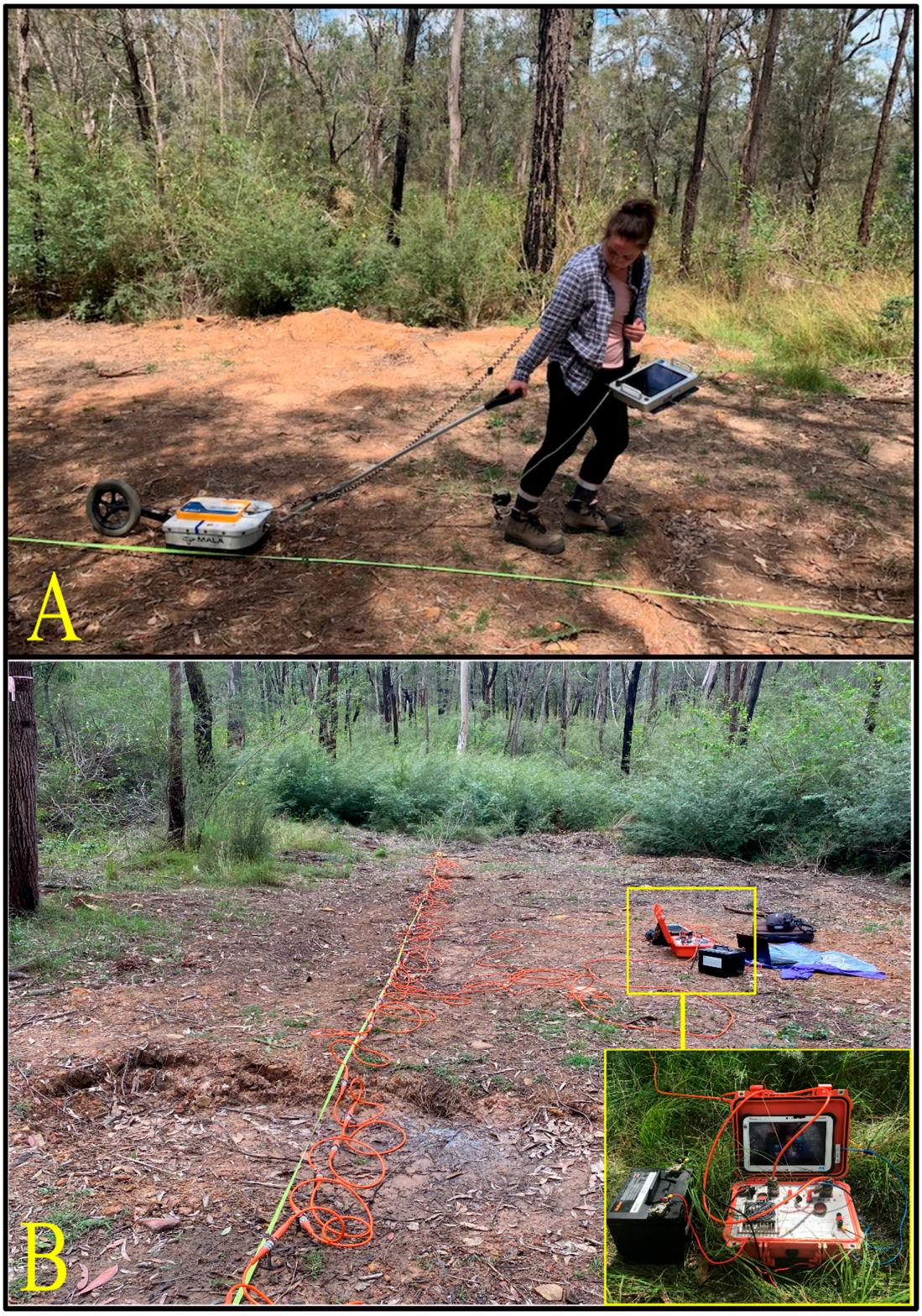

Figure 3. Geophysical techniques in use. (**A**) Mala X3M 500 MHz GPR system. This photo was previously published by Berezowski et al. [30] and is republished here with permission. (**B**) 64-electrode ZZ FlashRes 64 ERT system. This photo was partially published by Berezowski et al. [30] and is republished here with permission.

2.4. ERT Surveys

A ZZ FlashRes64 ERT system (see Figure 3B) was used, with survey parameters that include 64 electrodes at 0.25 m, Wenner (K = 20) and Dipole-Dipole (K = 15, L = 5) arrays, 120-voltage, and a 1.2/0.2 on/off time. Once the ERT lines were collected, the data were extracted using ZZ software (v. 4.0), transformed, filtered in R software (the R transformation and filtering steps are written and maintained by Associate Professor Dr Ian Moffat, and can be found on Github (Wenner array: https://github.com/IanMoffat/ZZ_ERT_Conversion/blob/main/ZZtoWenner.R (accessed on 21 November 2022) and Dipole-Dipole array: https://github.com/IanMoffat/ZZ_ERT_Conversion/blob/main/ZZtoDipoleDipole.R (accessed on 21 November 2022)), and then individually processed and inverted in Res2DInv. The Res2DInv inversions follow a least-squares (L1 robust) inversion approach [31] and were preceded by exterminating bad data points. The Dipole-Dipole data were processed using half-width cells (12.5 cm), and the Wenner data were processed using the full cell width (25 cm). To facilitate a meaningful comparison, the natural jenks breaks in the resistivity values of the six surveys were calculated using the getJenksBreaks function with the BAMMtools package in R, which generated a common resistivity scale for each array. These values were then input into Res2DInv, and each survey was re-displayed using the common resistivity scale.

The ERT data were also visualised with a resistivity difference plot, a plot created in Python (v. 3.11.5) that highlights the difference in the resistivity values between two chosen surveys. Difference plots reveal spatial changes that have occurred over time, thereby highlighting the processes of interest. This can be difficult when comparing two profiles at two given points in time. For this research specifically, two types of resistivity difference plots were created: (1) to demonstrate the differences in the resistivity values between the control (pre-burial) and all post-burial surveys (one, eight, fourteen, and twenty months post-burial)—these plots can demonstrate how different the resistivity values were at each survey point compared to when there was no grave; and (2) consecutive survey plots to see the changes in the resistivity values between adjacent surveys, i.e., pre-burial to post-burial, post-burial to one-month, one-month to eight-months, etc. These plots demonstrate the differences between two consecutive surveys and allow for a more in-depth analysis of how the climate and rainfall affects the resistivity values.

2.5. Soil Testing

Prior to the pig cadavers being placed in the graves, 10 soil samples were taken for further analysis, including grain size, magnetic susceptibility, and soil water content, organic and carbonate matter fractions (using Loss on Ignition [LOI]). For PS1, three soil samples were taken at 0.10 m, 0.20 m, and 0.50 m deep; for PM1, three soil samples were taken at 0.15 m, 0.25 m, and 0.60 m deep; and for PS2, four soil samples were taken at 0.10 m, 0.25 m, 0.60 m, and 1.50 m deep. Refer to Figure S25 for the soil properties at each of the depths in which a soil sample was taken. Prior to any soil analyses, each sample was homogenised by mortar and pestle grinding.

Each soil sample was analysed for its grain size distribution (see Section S3.1 in the Supplementary Materials). The sample was weighed, placed in an Endecott's sieve and shaker, and mechanically shaken for five minutes. The sieve consisted of eight levels, with decreasing particle-size meshes that follow the Wentworth scale [32]. The sample within each sieve was then individually weighed and documented. At the end, the individual weights were summed, and the percentage of each indicated particle-size interval was calculated.

To test the magnetic susceptibility, a portion of each of the samples was placed in a small plastic container, and then individually tested three times using a Bartington MS2B dual frequency sensor. See Section S3.2 in the Supplementary Materials for the approximate weight of each sample, the mean low- and high-frequency measurements, and mean frequency-dependent susceptibility percentage.

Samples were further investigated for soil water content, organic, and carbonate matter fractions. Organic matter fractions of each sample were determined using LOI undertaken

in five steps, using a modified version described by Heiri et al. [33]—see Section S3.3 in the Supplementary Materials for a more detailed description.

3. Results

The raw GPR and ERT data are available via Open Science Framework (https://doi.org/10.17605/OSF.IO/JCZWQ—[34]).

3.1. GPR Surveys

The profiles from the six GPR surveys are shown in Figure 4, with a summary of observations in Table 2. Note that dislocations to reflectors are non-continuous reflections that can be indicative of an anomaly (in this case, a grave-related anomaly).

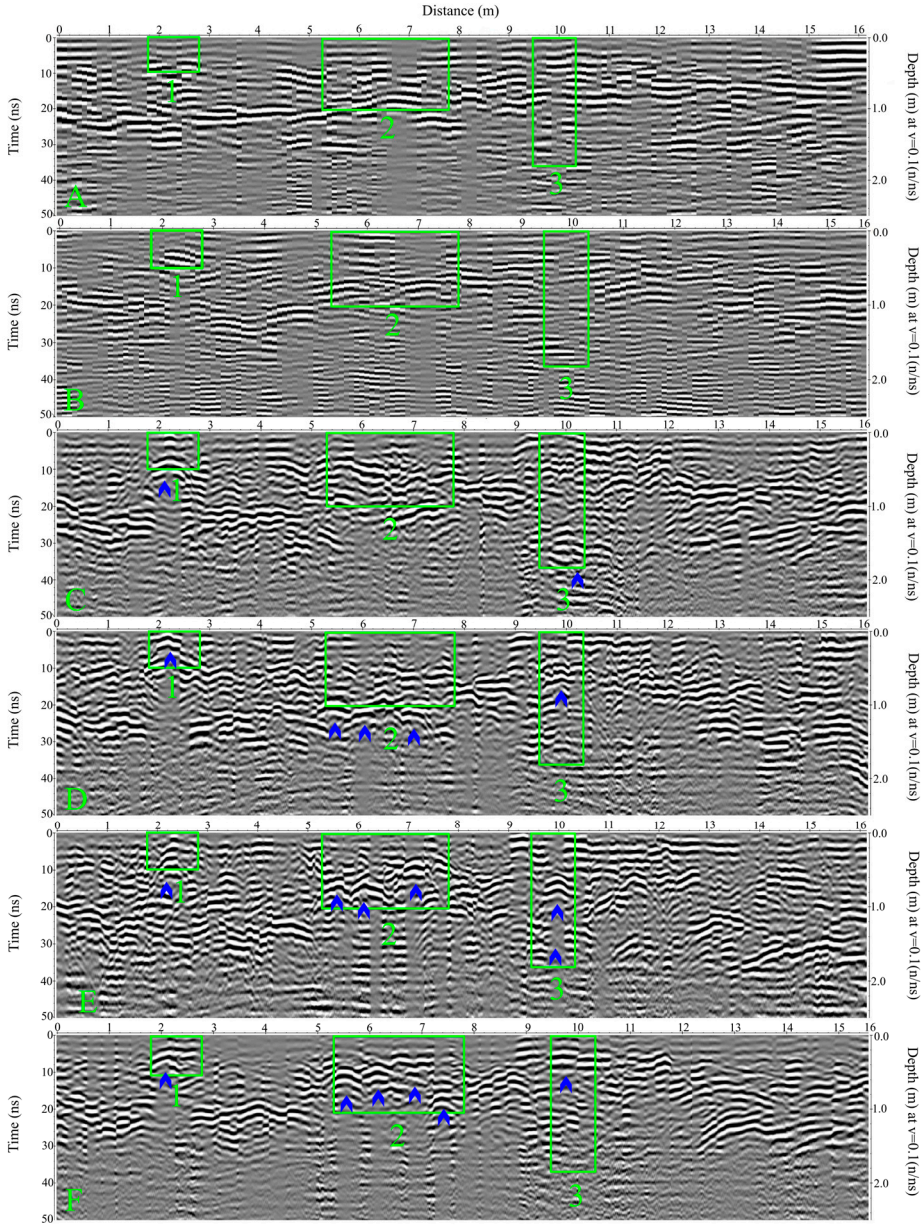

Figure 4. GPR profiles. GPR profiles from the pre-burial (**A**), post-burial (**B**), one-month (**C**), eight-month (**D**), fourteen-month (**E**), and twenty-month (**F**) surveys. The graves are denoted by a green rectangle; 1 is PS1, 2 is PM1, and 3 is PS2. Blue annotations highlight anomalies presented in Table 2. GPR profiles were processed in ReflexW.

Table 2. Summary of observations in the GPR profiles.

Survey Time in Relation to Pig Burial Creation (Letter in Figure 4) [mm-yy]	Summary of Observations		
	PS1	**PM1**	**PS2**
Pre-burial (A) [Mar-21]	No grave/control	No grave/control	No grave/control
Post-burial (B) [Mar-21]	Similar to (A)	Similar to (A)	Similar to (A)
One-month (C) [Apr-21]	Hyperbola with 0.09 ns velocity *	No clear grave-indicating anomaly; similar to surrounding soil	Dislocation to reflectors at base of grave; similar to surrounding soil up to 1 m deep
Eight-month (D) [Nov-21]	Dislocation in reflectors	Dislocations to reflectors at base of grave	Dislocation to reflectors; similar to surrounding soil up to 1 m deep
Fourteen-month (E) [May-22]	Hyperbola with 0.075 ns velocity *	Dislocations to reflectors	Dislocation to reflectors at surface, ~15 ns, and ~30 ns
Twenty-month (F) [Nov-22]	Dislocation to reflectors	Dislocation to reflectors	Dislocation to reflectors; similar to surrounding soil up to 1 m deep

* A single-layer velocity analysis of each hyperbola was conducted in ReflexW. The results can be found in Section S1.1 of the Supplementary Materials. Due to the homogeneous nature of the soil, the velocity analyses of the hyperbolae were only conducted on a single layer.

3.2. ERT Surveys

The profiles from the six ERT surveys are shown in Figure 5 (Dipole-Dipole) and Figure 6 (Wenner), with a summary of observations in Table 3.

Resistivity difference plots comparing the post-burial surveys to the control (pre-burial survey) were created and compared, with resistivity increases being shown in red and resistivity decreases being shown in blue. The results can be seen in Figure 7 (Dipole-Dipole) and Figure 8 (Wenner). Using the Dipole-Dipole data, the differences between the pre- and post-burial surveys (Figure 7a) are slight resistivity increases in the shallow subsurface (up to 1 m deep) of the three graves, with PM1 showing the largest increase. The non-grave areas, especially those deeper than 1 m, demonstrate very little change in the resistivity values; however, there is a small resistivity increase in the shallow subsurface around 13–14 m. In the pre-burial and one-month comparison (Figure 7b), the resistivity increases in PM1 changed to a resistivity decrease. PS1 is characterised mostly by a slight resistivity decrease; however, there is a large increase on the left grave wall. PS2 shows very slight resistivity increases and decreases as well; however, only up to 1 m deep. The non-grave areas are characterised by a resistivity increase in the shallow subsurface between PS1 and PM1, with a slight increase down the left edge of the profile, as well as a resistivity decrease in the shallow subsurface to the right of PS2. In the pre-burial and eight-month comparison (Figure 7c), the shallow subsurface of the grave areas are characterised by resistivity decreases. The non-grave areas are characterised by resistivity increases between and beneath the graves, as well as a resistivity decrease in the shallow subsurface to the right of PS2. In the pre-burial and fourteen-month comparison (Figure 7d), the graves are again characterised by resistivity decreases; however, the decrease seen in PS2 is very slight. In the non-grave areas, there are resistivity increases between and beneath the three graves and a resistivity decrease to the right of PS2. Finally, in the pre-burial and twenty-month comparison (Figure 7e), PS1 and PM1 are still characterised by a resistivity decrease; however, PS2 shows very little change. The non-grave areas are characterised by a resistivity increase between PS1 and PM1, a mixture of increases and decreases between PM1 and PS2, and a slight resistivity decrease to the right of PS2.

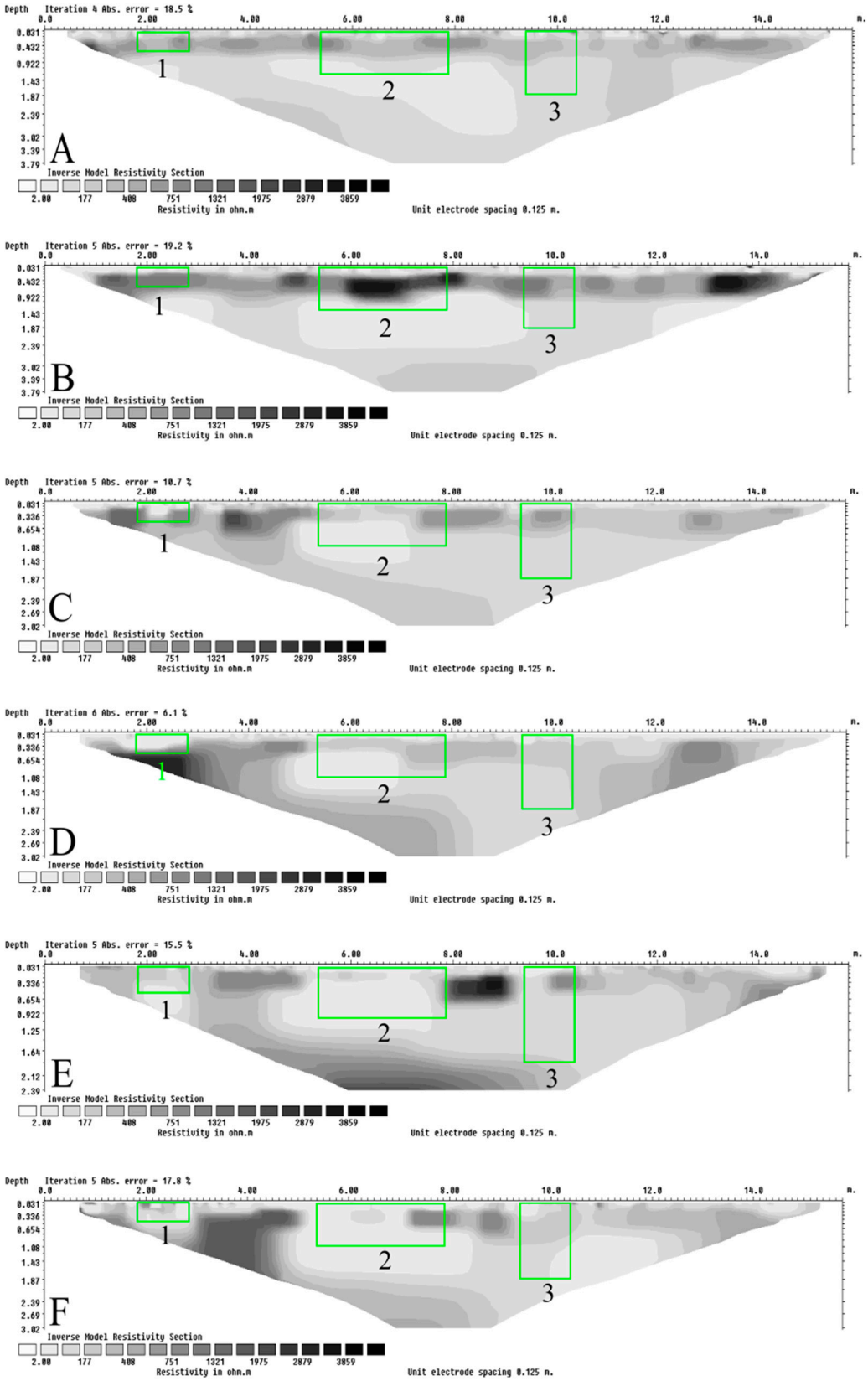

Figure 5. ERT profiles—Dipole-Dipole data. ERT profiles from the pre-burial (**A**), post-burial (**B**), one-month (**C**), eight-month (**D**), fourteen-month (**E**), and twenty-month (**F**) surveys for the Dipole-Dipole array. The graves are denoted by a green rectangle; 1 is PS1, 2 is PM1, and 3 is PS2. The ERT data were transformed in R, processed, and inverted in Res2DInv.

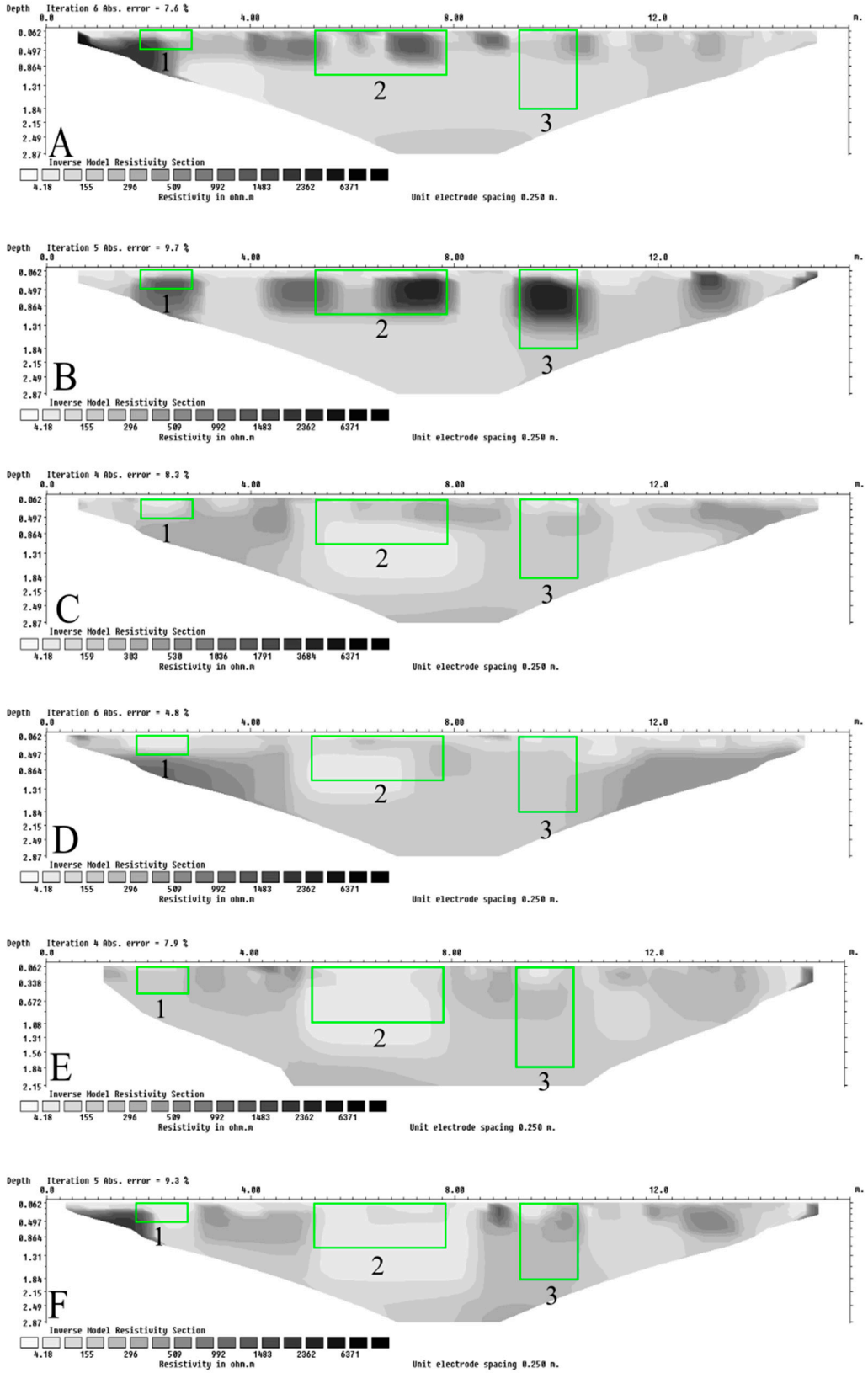

Figure 6. ERT profiles—Wenner data. ERT profiles from the pre-burial (**A**), post-burial (**B**), one-month (**C**), eight-month (**D**), fourteen-month (**E**), and twenty-month (**F**) surveys for the Wenner array. The graves are denoted by a green rectangle; 1 is PS1, 2 is PM1, and 3 is PS2. The ERT data were transformed in R, processed, and inverted in Res2DInv.

Table 3. Summary of observations in the ERT profiles.

Survey Time in Relation to Pig Burial Creation (Letter in Figures 5 and 6) [mm-yy]	**Summary of Observations**					
	PS1		**PM1**		**PS2**	
	Dipole-Dipole	**Wenner**	**Dipole-Dipole**	**Wenner**	**Dipole-Dipole**	**Wenner**
Pre-burial (A) [Mar-21]	No grave/control	No grave/control	No grave/control	No grave/control	No grave/control	No grave/control
Post-burial (B) [Mar-21]	No clearly observable grave anomalies	High-resistivity anomaly	High-resistivity anomaly in the centre of the grave area; low resistivity anomaly below the grave	High resistivity anomaly	No clearly observable grave anomalies	High resistivity anomaly
One-month (C) [Apr-21]	No clearly observable grave anomalies	Low resistivity anomaly	Low resistivity anomaly	Low resistivity anomaly	High resistivity anomaly near surface of the grave	No clearly observable grave anomalies
Eight-month (D) [Nov-21]	Low resistivity anomaly; similar to surrounding non-grave areas	Low resistivity anomaly	Low resistivity anomaly	Low resistivity anomaly	No clearly observable grave anomalies	No clearly observable grave anomalies
Fourteen-month (E) [May-22]	Low resistivity anomaly below grave floor	No clearly observable grave anomalies	Low resistivity anomaly	Low resistivity anomaly	No clearly observable grave anomalies	No clearly observable grave anomalies
Twenty-month (F) [Nov-22]	Non-uniform low resistivity anomaly	Low resistivity anomaly	Low resistivity anomaly	Low resistivity anomaly	No clearly observable grave anomalies	No clearly observable grave anomalies

High/low resistivity anomalies are noted when they are seen in the area of the grave and not in the surrounding soil.

Similar to the Dipole-Dipole data, the comparison between the pre- and post-burial surveys using the Wenner data (Figure 8a) demonstrates resistivity increases within the graves; however, there are resistivity decreases in the shallow subsurface (up to 1 m deep) of the non-grave areas. Interestingly, when comparing the one-, eight-, fourteen-, and twenty-month surveys to the pre-burial survey (Figure 8b–e, respectively), PS1 and PM1 are consistently characterised by a resistivity decrease, whereas PS2 shows very little changes. The non-grave areas also show very little changes, except for a slight resistivity increase in the eight- and fourteen-month comparisons (Figure 8c,d, respectively).

Consecutive resistivity difference plots were also created and compared. The results can be seen in Figure 9 (Dipole-Dipole) and Figure 10 (Wenner). For the Dipole-Dipole data, the difference between the pre- and post-burial surveys (Figure 9a) are most obvious in the grave areas, as shown by an increase in resistivity (red). When comparing the post-burial and one-month surveys (Figure 9b), the previously shown resistivity increases have transformed to resistivity decreases (blue). In the one- and eight-month survey comparison (Figure 9c), there are minimal resistivity decreases in the grave areas, and more resistivity increases directly under PS1, in the deep subsurface under PS2, and on the SW end of the survey line. In the eight- and fourteen-month survey comparison (Figure 9d), PS1 shows a resistivity increase, while PM1 and PS2 show a resistivity decrease (except for a small increase at the SW wall, between the surface and 0.5 m deep of PS2). Additionally, the previous resistivity increases seen under PS1 and on the SW end of the line are resistivity decreases, and the resistivity increase under PM1 is more pronounced. Finally, in the fourteen- and twenty-month surveys (Figure 9e), the resistivity differences within the graves have switched from the previous comparison (i.e., increase to a decrease, and vice versa). The resistivity difference in the non-grave areas have also switched, with the area under PS1 being a resistivity increase, the area under PM1 being a resistivity decrease, and the SW end of the line showing no changes.

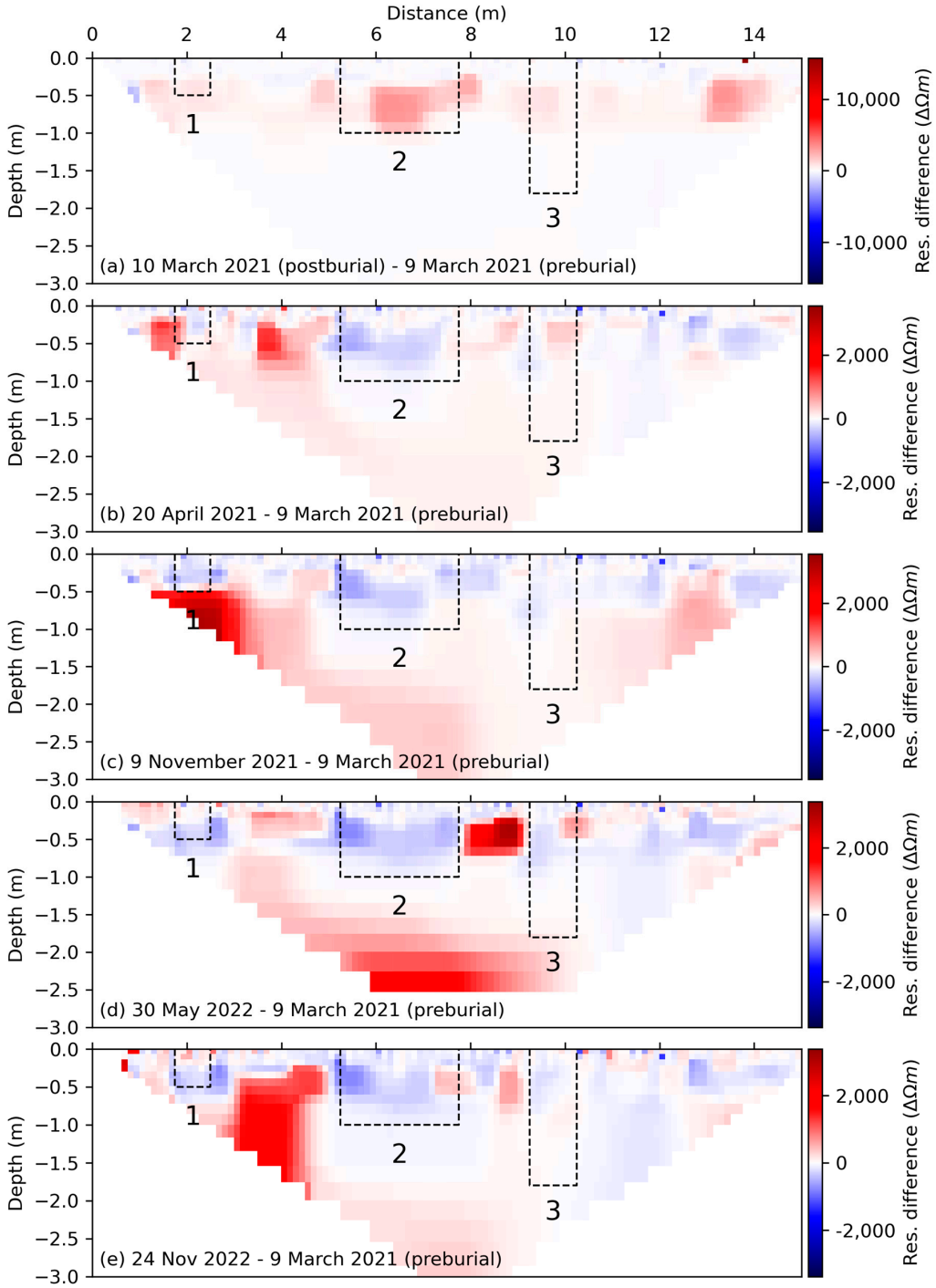

Figure 7. Resistivity difference plots between the pre-burial and all post-burial surveys. The immediate post-burial survey (**a**), as well as the one-month (**b**), eight-month (**c**), fourteen-month (**d**), and twenty-month (**e**) post-burial surveys. The red denotes a resistivity increase and the blue denotes a resistivity decrease. The graves are denoted by the black rectangles; 1 is PS1, 2 is PM1, and 3 is PS2. Dipole-Dipole data. Graphs generated in Python.

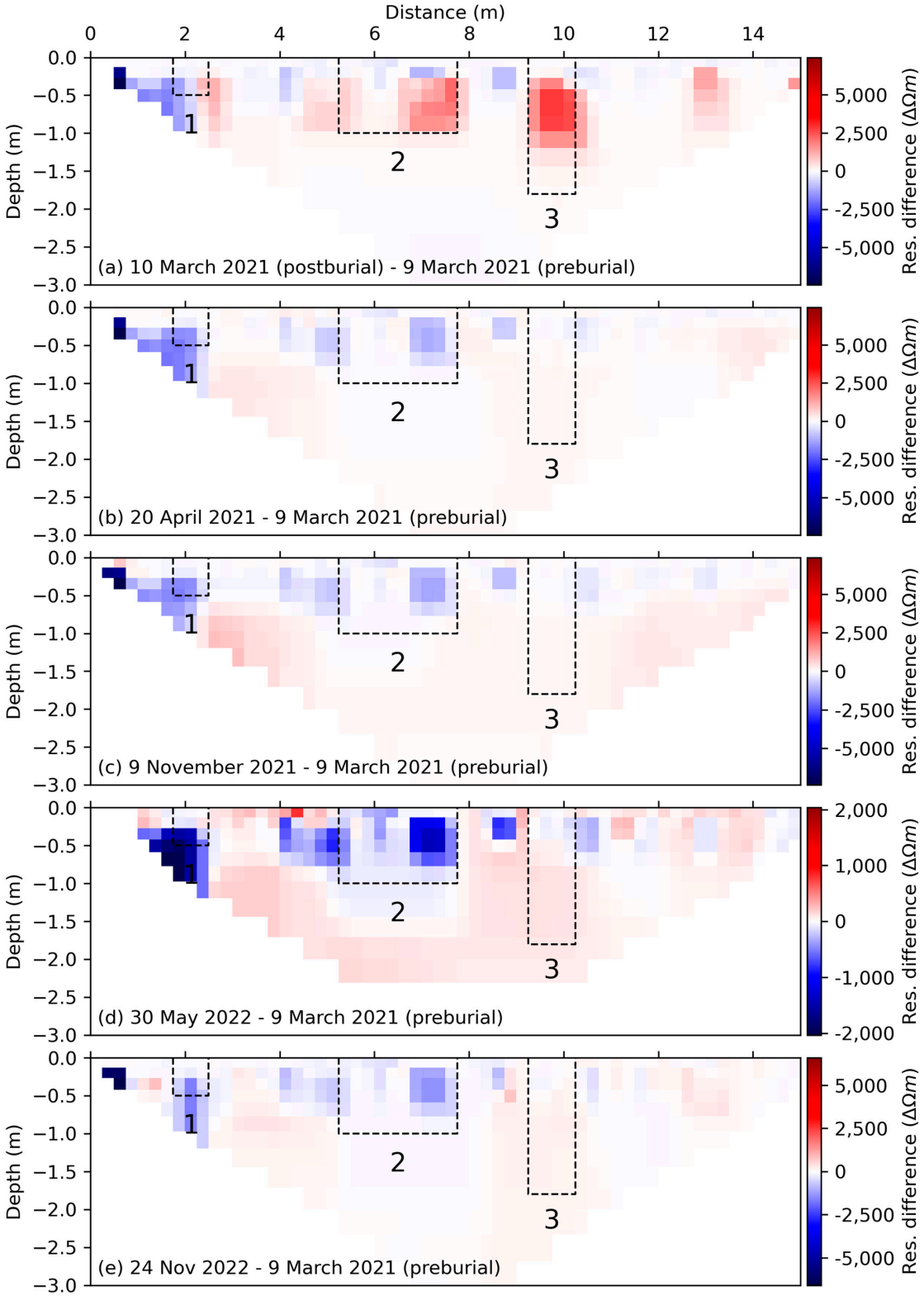

Figure 8. Resistivity difference plots between the pre-burial and all post-burial surveys. The immediate post-burial survey (**a**), as well as the one-month (**b**), eight-month (**c**), fourteen-month (**d**), and twenty-month (**e**) post-burial surveys. The red denotes a resistivity increase, and the blue denotes a resistivity decrease. The graves are denoted by the black rectangles; 1 is PS1, 2 is PM1, and 3 is PS2. Wenner data. Graphs generated in Python.

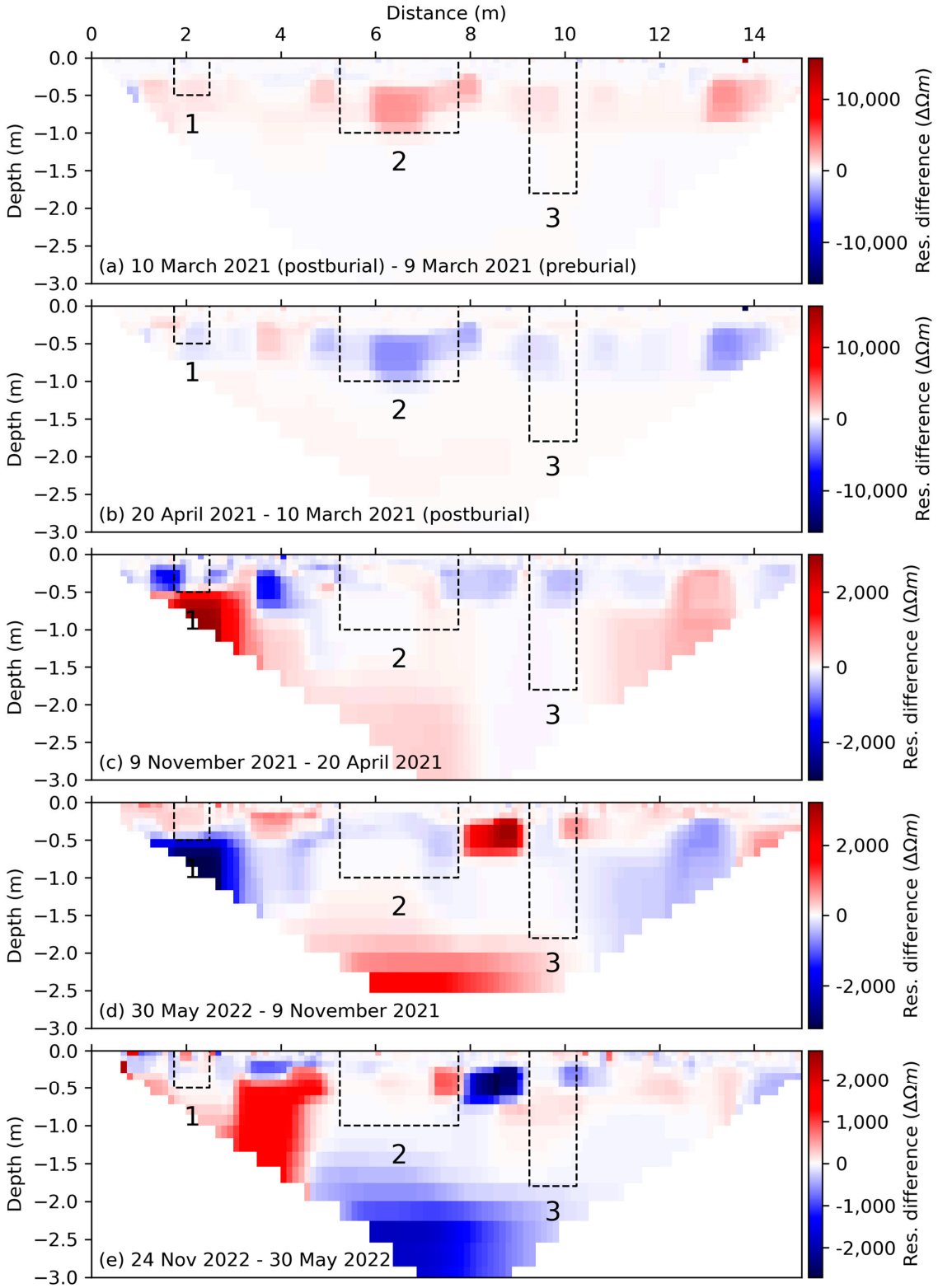

Figure 9. Resistivity difference plots between consecutive surveys. Post- and pre-burial (**a**), one-month and post-burial (**b**), eight- and one-month (**c**), fourteen- and eight-month (**d**), and twenty- and fourteen-month (**e**) surveys. The red denotes a resistivity increase, and the blue denotes a resistivity decrease. The graves are denoted by the black rectangles; 1 is PS1, 2 is PM1, and 3 is PS2. Dipole–Dipole data. Graphs generated in Python.

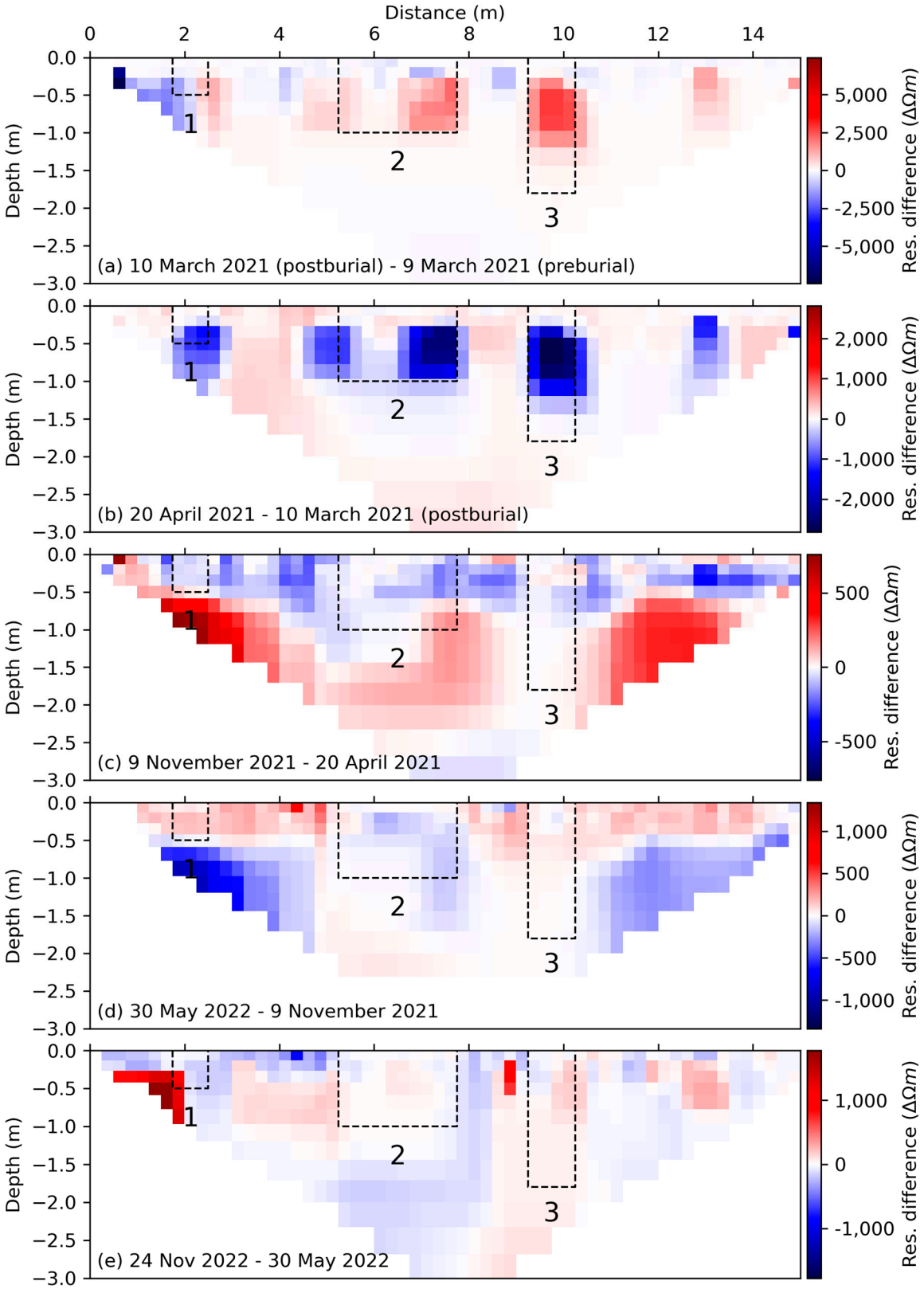

Figure 10. Resistivity difference plots between consecutive surveys. Post- and pre-burial (**a**), one-month and post-burial (**b**), eight- and one-month (**c**), fourteen- and eight-month (**d**), and twenty- and fourteen-month (**e**) surveys. The red denotes a resistivity increase, and the blue denotes a resistivity decrease. The graves are denoted by the black rectangles; 1 is PS1, 2 is PM1, and 3 is PS2. Wenner data. Graphs generated in Python.

For the Wenner data, the trends in the resistivity changes in the pre- and post-burial (Figure 10a) and the post-burial and one-month (Figure 10b) surveys mirror those of the Dipole-Dipole data; however, the increases/decreases are more pronounced. In the one- and eight-month comparison (Figure 10c), the grave areas highlight a resistivity decrease and the surrounding non-grave areas highlight a resistivity increase. In the eight- and fourteen-month comparison (Figure 10d), PS1 is highlighted by a resistivity increase, PM1 by resistivity decrease, and PS2 by a slight increase in the first 0.5 m followed by no changes to the base of the grave. The non-grave areas, especially those under PS1 and on the SW end of the survey line are highlighted by a resistivity decrease. Finally, the fourteen- and twenty-month comparison (Figure 10e) shows a resistivity decrease in PS1, a slight increase in PM1, and an increase in PS2. The non-grave areas show a mixture of both increases and decreases.

3.3. Soil Sample Testing

According to the grain size analysis, the soil mainly consists of fine and very fine-grained sand (59%), with small amounts of silt and clay (16%). Significant percentages of fine-grained gravel and above are present in the samples, interpreted to be saprolite, immediately above bedrock. The magnetic susceptibility and LOI analyses suggested a poorly developed soil profile (χfd% 1.7% in PS1 and PM1 and 3.1% in PS2 with very little organic material (an average of 5% in PS1, 5.2% in PM1, and 5.6% in PS2). For detailed results, including grain size, magnetic susceptibility, and loss on ignition, see Sections S3.1, S3.2 and S3.3, respectively, in the Supplementary Materials.

4. Discussion

4.1. Are the Graves Observable Using GPR and ERT?

The observability of the graves in Figures 4–6 is presented in Table 4. Observability in this instance is defined as the ability for the grave to be identified as an anomaly for further investigation (i.e., excavation) in a forensic case. Based on this, PM1 was the most observable grave by both GPR and ERT (this is important for humanitarian investigations involving the need to locate mass graves), followed by PS1 and PS2. When comparing the two techniques specifically, ERT was able to observe the graves more consistently than GPR. These results demonstrate that neither method reliably observed the graves under field conditions; however, the graves were observable by some of the techniques, some of the time. With the GPR, although the 500 MHz antenna was consistently able to penetrate at least 2 m for all surveys (due to the sandy nature of the soil), the observability of the graves was inconsistent. The shallow single grave (PS1) was the most consistently observed grave, followed by the mass grave (PM1), and then the deep single grave (PS2). First, PS1 was observable by hyperbolae and dislocations in reflectors from the one-month survey onwards. Next, PM1 was observable by dislocations to reflectors from the eight-month survey onwards; however, in the twenty-month survey, they are not clearly distinguishable from the surrounding soil. Finally, PS2 was most observable in the fourteen-month survey by dislocation to reflectors at the surface, ~15 ns, and ~30 ns. Although there were also dislocations to reflectors (at the one-, eight-, and twenty-month surveys) indicating the grave's presence, the geophysical response was similar to that of the surrounding non-grave areas, making the observability unclear. The lack of observability of PS2 could indicate that an increase in depth does not equate to an increase in visibility.

Table 4. Overall observability of the graves of GPR and ERT profiles.

	Geophysical Observability								
		PS1			PM1			PS2	
	GPR	ERT (DD)	ERT (W)	GPR	ERT (DD)	ERT (W)	GPR	ERT (DD)	ERT (W)
Pre-burial									
Post-burial									
One-month									
Eight-month									
Fourteen-month									
Twenty-month									

Green signifies that the grave was observable, red signifies that the grave was not observable, and yellow signifies that there was partial observability. Partial observability was chosen if the grave-related anomaly was not different enough from the surrounding soil to be chosen as a potential grave. Grey signifies that there was no grave to observe. These observations were made from Figures 4–6.

The inconsistency in observability with GPR is likely due to the poorly developed soil at the research site, as it lacks obvious depositional or pedogenic layering or sedimentary structures, as shown in Figure 11. The sediment analysis revealed that the soils are extremely homogeneous. The grain size is dominated by fine- to very-fine-grained sand, with minor clay and silt. Magnetic susceptibility values, particularly frequency dependence, suggest limited pedogenesis (soil formation) or anthropogenic enhancement at any stratigraphic level. The LOI shows that all samples are principally siliclastic sediment, with minor levels of organic material and no carbonate. No sedimentary structures were observed, suggesting that the sediment was deposited by in situ bedrock decomposition or sheetwash, or that the primary depositional fabric has been removed by bioturbation.

While a mostly sandy soil profile is beneficial for GPR penetration [35], because it allows for a greater depth penetration, the lack of stratigraphy or sedimentary structures results in a lack of observability of the graves. Simply put, graves are geophysically observable because of the stratigraphic breaks resulting from the creation of the grave; however, due to the lack of sedimentary structures or changes in lithology, there is no stratigraphy to break. When the geophysical observability in this experimental study is compared to those similarly conducted by Schultz et al. [13], Schultz [12], and Pringle and colleagues [17–19], the importance of pedogenesis, and thus distinguishable stratigraphic layers, within the soil becomes apparent. Firstly, the experimental studies conducted by Schultz and colleagues [13] and Schultz [12] in Florida, USA, reported that the soils were a Utisol type with two horizons, including a sand horizon up to one metre deep, followed by a clay horizon, and an Entisol type with mostly sand horizons, respectively, which resulted in the successful observation of the graves throughout the study period. The two distinct soil horizons resulted in observable graves (as dislocations to reflectors), as opposed to the soil at the current study site. Alternatively, although Pringle et al. [17–19] conducted experimental research on a study site with horizons of sandy loam and sandstone (in Staffordshire, UK), which is similar to the current study site, the top layers of rich organic topsoil resulted in the graves being observable with GPR.

Unlike similar experimental studies previously mentioned [17–19], where the graves were most commonly observable with hyperbolae, this experimental study lacked clear hyperbolae, except for in the one- and fourteen-month surveys of PS1. In general, a lack of hyperbolae is due to a lack of contrast in the dielectric permittivity of the subsurface materials [36]. In the current study, the rare presence of a hyperbola could indicate sufficient contrast between the soil and the pig cadaver, or because of the increase in water or decomposition fluids in the pore spaces compared to the surrounding soils. The former is potentially the reason for the hyperbola denoting PS1 in the one-month survey. After only one-month in the ground, the pig cadaver was likely intact, with few decompositional changes, and therefore, the dielectric permittivities of the pig cadaver would be different than that of the surrounding soil. The lack of hyperbolae in the eight-month survey and reappearance in the fourteen-month survey could be due to the progression in decom-

position. More specifically, decomposition could be progressed enough that the influx of decompositional fluids surrounding the pig, and thus filling the pore space, could be contrasting enough from the surrounding soil to create a hyperbola. However, there was also an increase in rainfall around the time of the fourteen-month survey and therefore, the increase in water in the pore space could also have provided sufficient contrast to create the hyperbola. A third explanation for this hyperbola could also be because the electromagnetic waves are reflecting off the chest cavity of the pig cadaver (supported by the lack of hyperbola in the twenty-month survey—see Section 4.2 for further explanation). Unfortunately, the research methods did not include site/grave-specific soil moisture monitoring, nor did it directly monitor decomposition of the pigs (i.e., the pigs were not excavated at any of the surveys), so a more specific explanation of the hyperbolae cannot be given.

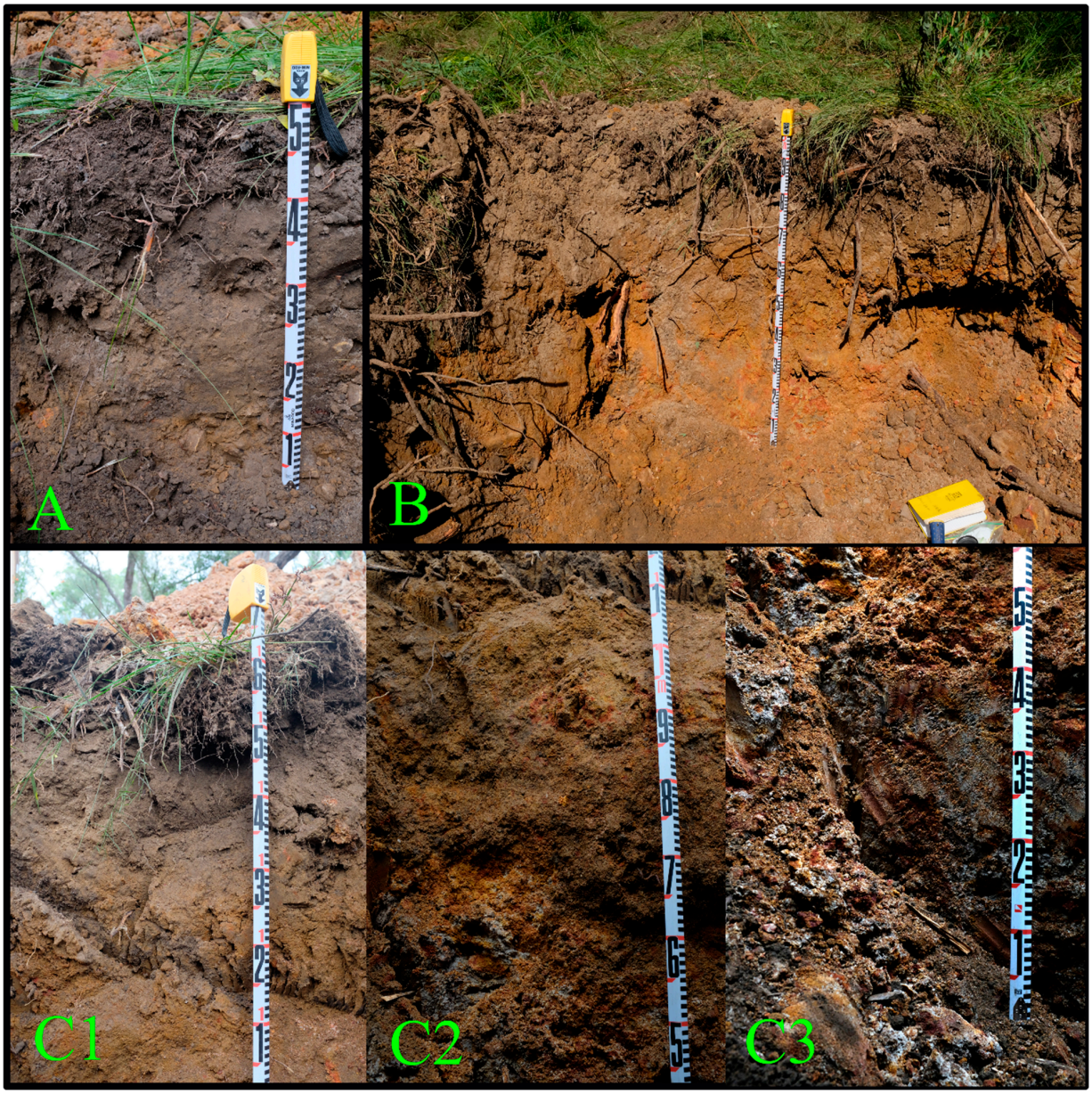

Figure 11. Soil profiles at AFTER animal site. Vertical soil profiles of PS1 ((**A**)—0–0.5 m), PM1 ((**B**)—0–1 m), and PS2 ((**C**)—(**C1**): 1–1.8 m; (**C2**): 0.5–1 m; (**C3**): 0–0.5 m) highlighting the lack of both pedogenic or sedimentary structures.

In the ERT profiles, PM1 was the most clearly observable grave, followed by PS1, and then PS2. First, PM1 was consistently observable as a large, low resistivity anomaly

from the one-month survey onwards, in both the Dipole-Dipole and Wenner arrays. This increased observability could be linked to the increase in volume (of disturbed soil within the grave). Next, PS1 was observable by a low resistivity anomaly from the one-month survey onwards with Wenner (with exception with the 14 months survey) and from the eight-month survey onwards with Dipole-Dipole (with exception to the fourteen-month survey where the low resistivity anomaly was below the grave floor and not throughout the grave). Finally, PS2 was not observable with either array, potentially highlighting that increased depth does not increase observability. This was also reported by Molina et al. [20]. The finding that the (naked) graves are observable by low resistivity anomalies is congruous with other published literature [3,11,14,17–19,27,29,37,38].

To further investigate the observability of the graves with ERT, difference plots that compare the pre- and post-burial surveys (Figures 7 and 8 for Dipole-Dipole and Wenner, respectively) were created. These graphs provide further evidence that ERT was successfully able to observe the graves, albeit inconsistently. More specifically, both Dipole-Dipole and Wenner arrays were able to observe the mass grave, as it was characterised by a consistent resistivity decrease; however, PS1 was only observable in the Dipole-Dipole data, and PS2 was not observable at all. Alternatively, the resistivity increases in the grave areas seen only in the pre- and immediate post-burial surveys (Figures 7a and 8a) are due to the grave creation process. As the post-burial graves are backfilled, and there was negligible rain, the pore space is larger and filled with air, which results in higher resistivity values. This increase in resistivity can also be seen in the ERT Wenner profile (Figure 6), where the three graves are highly visible by large circular high-resistivity anomalies. In Figure 8d, the comparison between the pre- and fourteen-month post-burial surveys, the resistivity decreases around PS1 and PM1 are larger than the resistivity decreases seen in the same areas of Figure 8c,e. This could be due to the increased rainfall between the eight- and fourteen-month survey periods (Figure 2, middle). Resistivity difference plots of every survey combination were also created to investigate the differences in resistivity values between each of the surveys—these can be found in Section S2.8 of the Supplementary Materials.

The Dipole-Dipole data of the whole grave and whole non-grave areas (Section S2.5 in the Supplementary Materials), excluding the pre- (no grave) and post-burial (discussed below in Section 4.2) surveys, shows that the difference between the two areas generally increases in observability with time, which could indicate that graves with a longer time-since-burial could be easier to observe geophysically. This trend could be explained by the progression of decomposition, as decomposition fluids can cause a decrease in the resistivity values [14]. This trend is also seen in PM1 with the Wenner data; however, it is not mirrored in PS1 with the Dipole-Dipole data, nor in the single graves with the Wenner data.

The differences in the grave and non-grave areas were further explored by graphing the changes in resistivity values with depth (Section S2.7 in the Supplementary Materials), which, in general, also demonstrated sufficient difference between the two areas. Interestingly, the resistivity values within the graves show a (relatively) consistent trend of a resistivity increase around 20–80 cm deep, regardless of the depth of the grave, where the pig is placed within the grave, and the hypothesised phase of decomposition.

The inconsistency in the grave's observability with ERT could be due to the unprecedented climate conditions experienced during the survey period. Between the pre-burial and twenty-month surveys, the Sydney area (NSW, Australia) experienced two anomalous rain events. According to the Bureau of Meteorology, the annual rainfall in 2021 and 2022 was 1047 mm and 1471 mm, respectively, which is 84% and 159% more than 2018 (568 mm), 118% and 206% more than 2019 (481 mm), and 47% and 107% more than 2020 (712 mm). This increased rain could have acted as a constant flush of any cadaver-related fluids, and any salts, that would decrease the resistivity values.

The anomalous rainfall also affected the resistivity values due to increased soil moisture. When the cumulative rainfall throughout the survey period was graphed against the whole grave resistivity values of the three graves (Section S2.3 in the Supplementary Materials), it showed that there was no correlation between the rainfall and the resulting resistivity. For

example, at the fourteen-month survey, the cumulative rainfall was at its highest (1229 mm) and the resulting resistivity values were low; however, the cumulative rainfall at the twenty-month survey is significantly lower (474 mm) and the resistivity values are still low. Similarly, when looking at the whole non-grave areas and the rainfall (Section S2.4 in the Supplementary Materials), the point of the highest average resistivity (fourteen-month survey) is also the point of the most cumulative rainfall. This is interesting because in general, an increase in rainfall should decrease resistivity [39]; however, due to the extensive amount of rain around the time of this survey (see Figure 2 [middle]—daily rain), the increase in resistivity could be due to the rain flushing out the salt (from decompositional fluids).

Alternatively, when the soil moisture was compared to the whole grave (Section S2.3 in the Supplementary Materials) and whole non-grave areas (Section S2.4 in the Supplementary Materials), we can see a correlation between the moisture and resulting resistivity values. For example, when the soil moisture is low the resistivity is higher (due to the air in the pore spaces) and when the soil moisture is high, the resistivity is lower (due to the water in the pore spaces). The exceptions to this trend are most noticeable in PM1 and PS2 at the eight-month survey, as the soil moisture values are low, but the resistivity values are also low. This could indicate that the cadaver may have been in an active state of decomposition, and the added decomposition fluids decreased the resistivity values.

To further investigate the resistivity changes in the non-grave areas, seven non-grave areas were selected and interpreted based on the rainfall and soil moisture data (Section S2.6 in the Supplementary Materials). In general, the mean resistivity values of the seven selective non-grave areas are not overly dependent on the rainfall and soil moisture. More specifically, in the Under PM1, PM1-PS2, and Under PS2 areas, which are the three areas with the same resistivity trend, peak at the point of the most cumulative rainfall, which is hypothetically when the resistivity values should be lower, as increased rainfall decreases resistivity. As discussed above, however, the large increase in rainfall could have flushed the salt (fluids associated with decomposition), thus resulting in increased resistivity values. Similarly, when compared with the soil moisture data, only 'Under PS1' and 'Post PS2' follow the appropriate resistivity/soil moisture trend, i.e., lower resistivity with higher soil moisture. Ultimately, these results show that the resistivity trends are different amongst the seven areas, and that they are not correlated to the climate, which is likely due to the unprecedented rainfall.

As both GPR and ERT were used concurrently, a comparison between the two techniques can be made. Interestingly, the GPR and ERT data did not always correlate. For example, in the fourteen-month GPR survey, the three graves are highly observable via hyperbola and dislocations to reflectors; however, in the ERT profile, only PM1 is obviously observable. As the observability in the fourteen-month GPR profile could be due to the electromagnetic waves reflecting off the chest cavities, this indicates that GPR and ERT respond to different subsurface matters. More specifically, as the lack of stratigraphy made it difficult for GPR to observe the soil changes, it relied on the cadavers; however, ERT could successfully detect the graves based on the soil disturbances related to creating a grave.

Ultimately, both GPR and ERT can be used as viable search techniques for covert burials; however, this research demonstrated that the soil and climate conditions play a big role in their success. If the soil and climate conditions permit, GPR and ERT can work well in succession, with GPR being used first to narrow down points of interest within a larger search area, followed by ERT, which can corroborate the location of a covert grave.

4.2. How Do the Geophysical Responses Change over Time?

Another facet of this project was to detail how the geophysical responses change over time. This is important because the victim(s) in homicide cases where a covert grave is used are not often found immediately, nor is there a consistent timeframe for when they are found. As such, having an improved understanding of what the geophysical responses look like from burial to 20-month post-burial can better guide these types of investigations.

With the GPR data, the grave-related anomalies become more observable with each subsequent survey (with exception to the twenty-month survey), which is likely due

to the process of decomposition aiding in their geophysical observability. The effects of decomposition are especially relevant when looking at the hyperbolae that indicate PS1, as well as the increased observability in the fourteen-month survey. First, there is a change in the hyperbola velocity from 0.09 ns at the one-month survey to 0.075 ns at the fourteen-month survey (see Section S1.1 in the Supplementary Materials). This could indicate that the cadaver is still in active decay at 14 months. Second, the three graves are most observable in the fourteen-month survey: PS1 by a hyperbola, and PM1 and PS2 by dislocations to reflectors that are not seen in the surrounding soil. These GPR anomalies could be from the electromagnetic waves directly reflecting off the pig cadavers, as opposed to the disturbed soil, indicating that the chest cavity is still intact at 14 months post-burial. Interestingly, these grave-related anomalies are not as obvious in the twenty-month survey, potentially indicating that the chest cavities have collapsed, and the electromagnetic waves are reflecting off the accompanying grave-related disturbances instead. This finding should be further confirmed with subsequent surveys. However, there were anomalous amounts of rain throughout the survey period, and therefore, the increased presence of water in the pore spaces of the disturbed graves could also explain the increased observability.

One of the biggest changes seen throughout the survey period was the increased resistivity values in the post-burial survey. This is evident when looking at the resistivity data, including in the post-burial survey of the Wenner array (Figure 6B), as well as when graphing the mean resistivity values of the whole grave areas (Section S2.3 in Supplementary Materials). In both the Dipole-Dipole and Wenner arrays, the post-burial survey shows high resistivity values, compared to the other five surveys. The reason for the large increase in the resistivity values is likely from the process of grave creation. To create the graves, the soil was removed, placed in large piles just adjacent to the graves and then placed back into the holes after the pigs were placed. This process caused immense disruption to the site and soil, inevitably increasing the resistivity values. These increased resistivity values were also reported by Doro et al. [23].

The Dipole-Dipole mean resistivity values of the pig, fill, and whole grave areas (graphically highlighted in Section S2 and further expanded on in Sections S2.1, S2.2 and S2.3, respectively, of the Supplementary Materials) follow a general downward trend as time progresses through the survey period (with exception with the resistivity increase in the post-burial survey, which was previously explained). This could be due to the pig cadavers progressing through decomposition, as the addition of decomposition fluids will cause a decrease in the resistivity values [14]; however, the progressive decrease in resistivity values can also be due to the progressive increase in rainfall and soil moisture. Alternatively, in the Wenner arrays, the resistivity values of the pig, fill, whole grave, and whole non-grave areas (Section S2 and further expanded on in Sections S2.1–S2.3, respectively, in the Supplementary Materials) are generally consistent throughout the survey period (again, not including the high post-burial resistivity value).

To further assess how the geophysical responses of the graves changed over time, resistivity difference plots of the consecutive surveys were created and analysed (Figures 9 and 10 for Dipole-Dipole and Wenner, respectively). Using the rainfall and soil moisture data, these results follow a textbook resistivity recording of water percolation through the vadose zone [40]. In the pre- and post-burial survey difference plot (Figure 9a for Dipole-Dipole and Figure 10a for Wenner), the non-grave areas are largely unchanged; however, because of the creation of the simulated graves just prior to the post-burial survey, the grave areas demonstrate a high resistivity difference, due to the larger pore space from the fill soil and the lack of rainfall. In the post-burial and one-month survey difference plot (Figure 9b for Dipole-Dipole and Figure 10b for Wenner), the non-grave areas are again largely unchanged; however, the grave areas demonstrate a low resistivity difference, explained by the soil moisture reaching field capacity (100%) just before/on the one-month survey date. This is explained by Archie's Law [41], which supports that the displacement of air with water causes a large change in resistivity. In the one- and eight-month survey difference plot (Figure 9c for Dipole-Dipole and Figure 10c for Wenner), there are high resistivity differences below 0.5 m, indicative of

dry deeper soils from a long period of low rainfall and soil moisture, and lower resistivity differences above 0.5 m, indicative of moist upper soil layers, from the fresh rainfall just prior to the eight-month survey. The eight- and fourteen-month survey difference plot (Figure 9d for Dipole-Dipole and Figure 10d for Wenner) then demonstrate the water percolating causing the upper soils to dry, indicative of low resistivity values below 0.5 m and high resistivity values above 0.5 m. The final difference plot, including the differences between the fourteen- and twenty-month surveys (Figure 9e for Dipole–Dipole and Figure 10e for Wenner), shows a mix of wet and dry soils due to the constant rain from La Niña.

Interestingly, the resistivity changes discussed above, which follow a traditional percolation through the vadose zone, are relatively absent in the grave areas. This could indicate that the pig cadavers act as an impervious 'percolation shield'. To the best of the authors' knowledge, this observation has not been made before. What this demonstrates is that rather than directly identifying graves, ERT allows indirect determination by observing an absence of water percolation through the vadose zone. To further confirm the fact that the pig cadavers may act as a percolation shield, ERT surveys would have to be continued, likely for at least another twelve-month period to understand the resistivity changes once the cadavers are skeletonised and thus no longer blocking the effects of percolation. Further, the authors recognise that the infiltration of water into the vadose zone is a transient process, and therefore there will be time lags between the rainfall and soil moisture; however, we do not have sufficient data to explore in the current project.

It is important to note that although the literature states that the fluids in the soil, including decomposition fluids, will affect the geophysical response [14,19,42], the interpretations made here from the geophysical data are based on general soil moisture readings from the area as well as the hypothesised decomposition stage of the buried pig cadavers. To accurately discuss the effect that the decomposition fluids would have on the geophysical responses, the pig cadavers needed to be excavated so that the decomposition state could be directly assessed. Additionally, although the anomalous increase in rainfall during the survey period was reflected in the general soil moisture readings, a more specific interpretation of the effect that an increase in moisture has on the geophysical responses could not be made without site/grave-specific soil moisture readings. Regardless, in the absence of the direct monitoring of fluids, other studies suggest that an increase in decomposition fluids decreases resistivity and can make the graves more observable with GPR [14,43]. To better understand how the progression of decomposition and the increase in rainfall affected the geophysical results, future research will focus on modelling Australian field conditions in both GPR and ERT modelling software.

5. Conclusions

Time-lapse GPR and ERT surveys were deployed to detect pig burials as a proxy for clandestine human graves. While GPR was successfully able to penetrate the depth of all three graves, the homogeneity of the soil (i.e., lack of stratigraphic layers) made it difficult to observe any stratigraphic breaks usually associated with covert graves. ERT was more successful under the study's anomalously wet climate conditions, with the largest (mass) grave being the most successfully observed. This finding is especially important in a humanitarian context, demonstrating that geophysical techniques can be used to locate mass graves related to violent conflict and/or political unrest. The deep single grave was the most difficult to observe with both GPR and ERT, demonstrating that an increased grave depth does not increase observability. The ERT responses over time revealed that the pig cadavers act as an impervious 'percolation shield', affecting resistivity changes related to water percolation. There was a general correlation between soil moisture and resistivity values, where high soil moisture resulted in lower resistivity values and vice versa. However, in areas with decomposing cadavers, the resistivity values decreased despite low soil moisture, likely due to the presence of decomposition fluids influencing the resistivity measurements.

When comparing GPR and ERT, their observations did not always correlate, with ERT successfully detecting graves based on soil disturbances, whereas GPR relied on reflections from cadavers. The study demonstrated that ERT is more universally effective in homogenous soil and wet climate conditions, making it a preferred choice for covert grave detection. However, both methods can be used in succession to corroborate grave locations if the soil and climate conditions allow. This supports the notion that a multidisciplinary technique can be beneficial when searching for clandestine graves (see [3,42,44,45]). This is significant as GPR has traditionally been the preferred method, but this research highlights the advantages of incorporating ERT for improved detection accuracy. As success is dependent on the soil and climate conditions, an extensive site history is vital before undertaking any geophysical surveys.

Considering that this project is the first time-lapse geophysical study investigating the observability of covert graves in Australia, the results can be used as a starting point for future research projects under Australian field conditions—especially because the success of both GPR and ERT depend on the soil and climate conditions. In future studies, certain aspects of the research design could be changed to allow for a deeper investigation into the factors affecting the geophysical responses. Firstly, although not collecting the GPR data in a grid was specifically chosen to accomplish the aims of this project, the GPR data in future studies can be collected using a grid. Secondly, to allow for a more nuanced discussion on how decomposition fluids affect the geophysical responses, a pig cadaver can be excavated at each survey time, noting that this will increase the time spent on scene and the resources needed. Finally, future studies could include a weather station and soil moisture metre directly on site, allowing for a more in-depth discussion on how the site-specific soil and climate conditions affect the geophysical responses. However, it should be noted that the presence of a soil moisture metre in the research area could influence the geophysical responses.

The study emphasised the complexities involved in interpreting resistivity values in geophysical surveys for grave detection. It underscored the considerable impact of factors like soil homogeneity, climate conditions, water percolation, and the presence of decomposing organic material on resistivity and permittivity values. As such, these factors warrant careful consideration in future research on geophysical surveys for grave detection.

Supplementary Materials: The following supporting information can be downloaded at: https://www.mdpi.com/article/10.3390/rs16183498/s1, Figure S1. Velocity analysis of the hyperbolae denoting PS1 seen in the one-month (A), and 14-month (B) surveys. GPR profiles were processed, and the hyperbolae were fitted in ReflexW.; Figure S2. Resistivity value inversion diagrams—visualization of the relevant areas of interest. The mean of each of the above areas were utilized to compare the resistivity values throughout the survey period. Diagram not to scale; Table S1. Locations of the graves along survey line; Figure S3. Mean resistivity values for the pig (A), fill (B), whole grave (C), and whole non-grave (D) portions of the ERT line throughout the survey period. Dipole-Dipole array; Figure S4. Mean resistivity values for the pig (A), fill (B), whole grave (C), and whole non-grave (D) portions of the ERT line throughout the survey period. Wenner array; Table S2. Mean resistivity values of the pig areas; Table S3. Mean resistivity values of the fill areas; Table S4. Mean resistivity values of the whole grave areas; Figure S5. Comparing the whole grave resistivity values of PS1, PM1, and PS2 to A) cumulative rainfall and B) shallow (0–1 m) and deep (1–6 m) soil moisture percentages. Dipole-Dipole data. The rainfall and soil moisture data were sourced from The Bureau of Meteorology; Figure S6. Comparing the whole grave resistivity values of PS1, PM1, and PS2 to A) cumulative rainfall and B) shallow (0–1 m) and deep (1–6 m) soil moisture percentages. Wenner data. The rainfall and soil moisture data were sourced from The Bureau of Meteorology; Table S5. Mean resistivity values of the whole non-grave area; Figure S7. Comparing the resistivity values of the whole non-grave area to A) cumulative rainfall and B) shallow (0–1 m) and deep (1–6 m) soil moisture percentages. Dipole-Dipole data. The rainfall and soil moisture data were sourced from The Bureau of Meteorology; Figure S8. Comparing the resistivity values of the whole non-grave area to A) cumulative rainfall and B) shallow (0–1 m) and deep (1–6m) soil moisture percentages. Wenner data. The rainfall and soil moisture data were sourced from The Bureau of Meteorology; Figure S9. Comparison between the whole grave resistivity values of PS1, PM1, and PS2 and the whole

non-grave (WNG) resistivity values. Dipole-Dipole array; Figure S10. Comparison between the whole grave resistivity values of PS1, PM1, and PS2 and the whole non-grave (WNG) resistivity values. Wenner array; Table S6. Percentage differences in mean resistivity values of the whole grave and whole non-grave areas; Figure S11. Resistivity inversion diagram denoting the selective non-grave areas for further analysis. Diagram not to scale; Figure S12. Selective non-grave areas, including Pre PS1 (1), Under PS1 (2), PS1-PM1 (2), and Under PM1 (4), graphed against the cumulative rainfall (A) and the soil moisture data (B). Dipole-Dipole data. Both the rainfall and soil moisture data were sourced from The Bureau of Meteorology; Figure S13. Selective non-grave areas, including PM1-PS2 (5), Under PS2 (6), and Post PS2 (7), graphed against the cumulative rainfall (A) and the soil moisture data (B). Dipole-Dipole data. Both the rainfall and soil moisture data were sourced from The Bureau of Meteorology; Figure S14. Selective non-grave areas, including Pre PS1 (1), Under PS1 (2), PS1-PM1 (2), and Under PM1 (4), graphed against the cumulative rainfall (A) and the soil moisture data (B). Wenner data. Both the rainfall and soil moisture data were sourced from The Bureau of Meteorology; Figure S15. Selective non-grave areas, including PM1-PS2 (5), Under PS2 (6), and Post PS2 (7), graphed against the cumulative rainfall (A) and the soil moisture data (B). Wenner data. Both the rainfall and soil moisture data were sourced from The Bureau of Meteorology; Figure S16. Resistivity value inversion diagram denoting the change with depth measurements through the midpoint of PS1, PM1, and PS2, as well as two non-grave areas. Diagram not to scale; Figure S17. Changes in the resistivity values with depth of the grave and non-grave areas. (1) pre-burial, (2) post-burial, (3) Apr-21, (4) Nov-21, (5) May-22, and (6) Nov-22. (A) PS1, (B) PM1, and (C) PS2. Dipole-Dipole data; Figure S18. Changes in the resistivity values with depth of the grave and non-grave areas. (1) pre-burial, (2) post-burial, (3) Apr-21, (4) Nov-21, (5) May-22, and (6) Nov-22. (A) PS1, (B) PM1, and (C) PS2. Please note the scale difference in 2C, as there were some resistivity values well above 1500, however, homogenizing the rest of the profiles to a 3000 Ωm scale would cause a loss of trend visibility. Wenner data; Figure S19. Resistivity difference plots between (a) post-burial and pre-burial, (b) Apr-21 and pre-burial, (c) Nov-21 and pre-burial, (d) May-22 and pre-burial, and (e) Nov-22 and pre-burial. Red represents an increase and blue represents a decrease in resistivity between two surveys. Dipole-Dipole data. Difference plots were generated in Python; Figure S20. Resistivity difference plots between (f) Apr-21 and post-burial, (g) Nov-21 and post-burial, (h) May-22 and post-burial, and i) Nov-22 and post-burial. Red represents an increase and blue represents a decrease in resistivity between two surveys. Dipole-Dipole data. Difference plots were generated in Python; Figure S21. Resistivity difference plots between (j) Nov-21 and Apr-21, (k) May-22 and Apr-21, (l) Nov-22 and Apr-21, (m) May-22 and Nov-21, (n) Nov-22 and Nov-21, and (o) Nov-22 and May-22. Red represents an increase and blue represents a decrease in resistivity between two surveys. Dipole-Dipole data. Difference plots were generated in Python; Figure S22. Resistivity difference plots between (a) post-burial and pre-burial, (b) Apr-21 and pre-burial, (c) Nov-21 and pre-burial, (d) May-22 and pre-burial, and (e) Nov-22 and pre-burial. Red represents an increase and blue represents a decrease in resistivity between two surveys. Wenner data. Difference plots were generated in Python; Figure S23. Resistivity difference plots between (f) Apr-21 and post-burial, (g) Nov-21 and post-burial, (h) May-22 and post-burial, and (i) Nov-22 and post-burial. Red represents an increase and blue represents a decrease in resistivity between two surveys. Wenner data. Difference plots were generated in Python; Figure S24. Resistivity difference plots between (j) Nov-21 and Apr-21, (k) May-22 and Apr-21, (l) Nov-22 and Apr-21, (m) May-22 and Nov-21, (n) Nov-22 and Nov-21, and (o) Nov-22 and May-22. Red represents an increase and blue represents a decrease in resistivity between two surveys. Wenner data. Difference plots were generated in Python; Figure S25. Soil profile at each depth (denoted by a green arrow) that a soil sample was taken from PS1 (A), PM1 (B), and PS2 (C1, C2, and C3); Table S7. Soil sample weights at each grave depth prior to grain size analysis; Figure S26. Grain size analysis results for the soil samples taken at the respective grave depths for PS1 (A), PM1 (B), and PS2 (C); Table S8. Grain size results for PS1; Table S9. Grain size analysis for PM1; Table S10. Grain size analysis of PS2; Figure S27. Magnetic susceptibility results. Low frequency (LF), high frequency (HF), and frequency-dependent susceptibility (FD%) for PS1 (A), PM1 (B), and PS2 (C); Figure S27. Magnetic susceptibility results. Low frequency (LF), high frequency (HF), and frequency-dependent susceptibility (FD%) for PS1 (A), PM1 (B), and PS2 (C); Figure S28. Loss on ignition results. Soil water content, organic, and carbonate matter fractions for PS1 (1A), PM1 (1B), and PS2 (1C), and the percentage of the total weight for each category for PS1 (2A), PM1 (2B), and PS2 (2C); Table S12. Loss on ignition results demonstrating the soil water content, organic, and carbonate matter fractions of PS1, PM1, and PS2. Reference [46] are cited in the Supplementary Materials.

Author Contributions: Conceptualization, V.B., X.M. and I.M.; data curation, V.B.; formal analysis, V.B. and G.C.R.; funding acquisition, V.B., X.M., D.S., I.C. and I.M.; investigation, V.B., X.M., D.S., I.C. and I.M.; methodology, V.B. and I.M.; resources, I.M.; software, I.M.; supervision, X.M., J.E. and I.M.; visualization, V.B. and G.C.R.; writing—original draft, V.B., X.M., D.S., I.C., J.E., G.C.R. and I.M.; writing—review and editing, V.B., X.M., D.S., I.C., J.E., G.C.R. and I.M. All authors have read and agreed to the published version of the manuscript.

Funding: This research was funded by a University of Newcastle Vice Chancellor's Higher Degree by Research PhD Training scholarship (Victoria Berezowski), a Doctoral Fellowship from the Social Sciences and Humanities Research Council of Canada #751-2021-0039 (Victoria Berezowski), a Flinders University Research Investment fund (Associate Professor Ian Moffat), an Australian Research Council LIEF grant #LE210100037 (Associate Professors Ian Moffat and Xanthé Mallett), an Australian Research Council DECRA (#DE160100703) and Future Fellowships (#FT220100184—Associate Professor Ian Moffat), a University of Newcastle Strategic Engagement Scheme Scholarship (Isabella Crebert), and an Emma Louise Kessler Grant (Dilan Seckiner).

Institutional Review Board Statement: Ethics approval for the project was obtained by The University of Newcastle (Animal Care and Ethics Committee), the University of Technology Sydney (UTS), and AFTER. Guidelines for the ethical use of pig cadavers was followed throughout all aspects of this project.

Data Availability Statement: The raw GPR and ERT data are available via Open Science Framework (https://doi.org/10.17605/OSF.IO/JCZWQ).

Acknowledgments: The authors would like to thank the Australian Facility for Taphonomic Experimental Research (AFTER) for the space and resources to conduct this project, Marc Young from Flinders University for assistance with the soil analyses, and the funding sources listed.

Conflicts of Interest: The authors declare no conflicts of interest.

References

1. Keatley, D.; O'Donnell, C.; Chapman, B.; Clarke, D.D. The psycho-criminology of burial sites: Developing the winthropping method for locating clandestine burial sites. *J. Police Crim. Psychol.* **2021**, *37*, 91–100. [CrossRef]
2. Ferguson, C. Forensically aware offenders and homicide investigations: Challenges, opportunities and impacts. *Aust. J. Forensic Sci.* **2019**, *51*, S128–S131. [CrossRef]
3. Berezowski, V.; Moffat, I.; Shendryk, Y.; MacGregor, D.; Ellis, J.; Mallett, X. A multidisciplinary approach to locating clandestine gravesites in cold cases: Combining geographic profiling, LiDAR, and near surface geophysics. *Forensic Sci. Int. Synerg.* **2022**, *5*, 100281. [CrossRef] [PubMed]
4. National Missing Persons Coordination Centre. *Missing Persons*; Australian Federal Police (AFP): Canberra, ACT, Australia, 2021.
5. Ferguson, C.; Pooley, K. Australian no-body homicides: Exploring common features of solved cases. *J. Forensic Leg. Med.* **2019**, *66*, 70–78. [CrossRef]
6. Ferguson, C.; Pooley, K. Comparing solved and unsolved no-body homicides in Australia: An exploratory analysis. *Homicide Stud.* **2019**, *23*, 381–403. [CrossRef]
7. Hinkes, M. Forensic anthropology in cold cases. In *Cold Case Homicides: Practical investigative Techniques*, 2nd ed.; Walton, R.H., Ed.; CRC Press: Boca Raton, FL, USA, 2017; pp. 381–400.
8. Donnelly, L.; Harrison, M. Geoforensic Search Strategy (GSS): Ground searches related to homicide graves, counter-terrorism and serious and organized crime. In *A Guide to Forensic Geology*; Geological Society: London, UK, 2021.
9. Reynolds, J.M. *An Introduction to Applied and Environmental Geophysics*; John Wiley & Sons: West Sussex, UK, 2011.
10. Telford, W.M.; Geldart, L.; Sheriff, R.E. *Applied Geophysics*; Cambridge University Press: Cambridge, UK, 1990.
11. Berezowski, V.; Mallett, X.; Ellis, J.; Moffat, I. Using ground penetrating radar and resistivity methods to locate unmarked graves: A review. *Remote Sens.* **2021**, *13*, 2880. [CrossRef]
12. Schultz, J.J. Sequential monitoring of burials containing small pig cadavers using ground penetrating radar. *J. Forensic Sci.* **2008**, *53*, 279–287. [CrossRef] [PubMed]
13. Schultz, J.J.; Collins, M.E.; Falsetti, A.B. Sequential monitoring of burials containing large pig cadavers using ground-penetrating radar. *J. Forensic Sci.* **2006**, *51*, 607–616. [CrossRef]
14. Jervis, J.R.; Pringle, J.K.; Tuckwell, G.W. Time-lapse resistivity surveys over simulated clandestine graves. *Forensic Sci. Int.* **2009**, *192*, 7–13. [CrossRef]
15. Damiata, B.N.; Steinberg, J.M.; Bolender, D.J.; Zoëga, G. Imaging skeletal remains with ground-penetrating radar: Comparative results over two graves from Viking Age and Medieval churchyards on the Stóra-Seyla farm, northern Iceland. *J. Archaeol. Sci.* **2013**, *40*, 268–278. [CrossRef]

16. Powell, K. Detecting buried human remains using near-surface geophysical instruments. *Explor. Geophys.* **2004**, *35*, 88–92. [CrossRef]
17. Pringle, J.K.; Jervis, J.R.; Hansen, J.D.; Jones, G.M.; Cassidy, N.J.; Cassella, J.P. Geophysical Monitoring of Simulated Clandestine Graves Using Electrical and Ground-Penetrating Radar Methods: 0–3 Years After Burial. *J. Forensic Sci.* **2012**, *57*, 1467–1486. [CrossRef]
18. Pringle, J.K.; Jervis, J.R.; Roberts, D.; Dick, H.C.; Wisniewski, K.D.; Cassidy, N.J.; Cassella, J.P. Long-term Geophysical Monitoring of Simulated Clandestine Graves using Electrical and Ground Penetrating Radar Methods: 4–6 Years After Burial. *J. Forensic Sci.* **2016**, *61*, 309–321. [CrossRef] [PubMed]
19. Pringle, J.K.; Stimpson, I.G.; Wisniewski, K.D.; Heaton, V.; Davenward, B.; Mirosch, N.; Spencer, F.; Jervis, J.R. Geophysical monitoring of simulated homicide burials for forensic investigations. *Sci. Rep.* **2020**, *10*, 7544. [CrossRef]
20. Molina, C.M.; Pringle, J.K.; Saumett, M.; Evans, G.T. Geophysical monitoring of simulated graves with resistivity, magnetic susceptibility, conductivity and GPR in Colombia, South America. *Forensic Sci. Int.* **2016**, *261*, 106–115. [CrossRef]
21. Cavalcanti, M.M.; Rocha, M.P.; Blum, M.L.B.; Borges, W.R. The forensic geophysical controlled research site of the University of Brasilia, Brazil: Results from methods GPR and electrical resistivity tomography. *Forensic Sci. Int.* **2018**, *293*, 101.e1–101.e21. [CrossRef] [PubMed]
22. Doro, K.O.; Kolapkar, A.M.; Bank, C.-G.; Wescott, D.J.; Mickleburgh, H.L. Geophysical imaging of buried human remains in simulated mass and single graves: Experiment design and results from pre-burial to six months after burial. *Forensic Sci. Int.* **2022**, *335*, 111289. [CrossRef]
23. Doro, K.O.; Emmanuel, E.D.; Adebayo, M.B.; Bank, C.-G.; Wescott, D.J.; Mickleburgh, H.L. Time-lapse electrical resistivity tomography imaging of buried human remains in simulated mass and individual graves. *Front. Environ. Sci.* **2022**, *10*, 882496. [CrossRef]
24. NSW Office of Environment and Heritage. NSW Soil and Land Information System (SALIS) Database. 2012. Available online: https://datasets.seed.nsw.gov.au/dataset/nsw-soil-profiles15bf7 (accessed on 22 November 2022).
25. Department of Planning, Industry and Environment. Australian Soil Classification (ASC) Soil Type map of NSW. 2021. Available online: https://datasets.seed.nsw.gov.au/dataset/australian-soil-classification-asc-soil-type-map-of-nsweaa10 (accessed on 22 November 2022).
26. Moffat, I. Locating graves with geophysics. In *Best Practices of Geoinformatic Technologies for the Mapping of Archaeolandscapes*; Archaeopress Archaeology: Oxford, UK, 2015; pp. 45–53. [CrossRef]
27. Pringle, J.K.; Jervis, J.; Cassella, J.P.; Cassidy, N.J. Time-lapse geophysical investigations over a simulated urban clandestine grave. *J. Forensic Sci.* **2008**, *53*, 1405–1416. [CrossRef]
28. Berezowski, V.; Mallett, X.; Simyrdanis, K.; Kowlessar, J.; Bailey, M.; Moffat, I. Ground penetrating radar and electrical resistivity tomography surveys with a subsequent intrusive investigation in search for the missing Beaumont children in Adelaide, South Australia. *Forensic Sci. Int.* **2024**, *357*, 111996. [CrossRef]
29. Berezowski, V.; Moffat, I.; Seckiner, D.; Crebert, I.; Ellis, J.; Mallett, X. The suitability of using domestic pigs (Sus spp.) as human proxies in the geophysical detection of clandestine graves. *J. Forensic Sci.* **2023**, *69*, 316–328. [CrossRef] [PubMed]
30. Berezowski, V.; Mallett, X.; Crebert, I.; Seckiner, D.; Ellis, J.; Moffat, I. A technical protocol for using ground penetrating radar and electrical resistivity tomography in the search for covert graves. *Aust. J. Forensic Sci.* **2023**, *56*, 534–550. [CrossRef]
31. Loke, M.H.; Barker, R.D. Least-squares deconvolution of apparent resistivity pseudosections. *Geophysics* **1995**, *60*, 1682–1690. [CrossRef]
32. Wentworth, C.K. A Scale of Grade and Class Terms for Clastic Sediments. *J. Geol.* **1922**, *30*, 377–392. [CrossRef]
33. Heiri, O.; Lotter, A.F.; Lemcke, G. Loss on ignition as a method for estimating organic and carbonate content in sediments: Reproducibility and comparability of results. *J. Paleolimnol.* **2001**, *25*, 101–110. [CrossRef]
34. Berezowski, V.; Mallett, X.; Seckiner, D.; Crebert, I.; Ellis, J.; Rau, G.C.; Moffat, I. Data Associated with "Comparison of Time-Lapse Ground-Penetrating Radar and Electrical Resistivity Tomography for Detecting Clandestine Graves Using Pigs". Open Science Framework. 2023. [CrossRef]
35. Schultz, J.J. Using ground-penetrating radar to locate clandestine graves of homicide victims: Forming forensic archaeology partnerships with law enforcement. *Homicide Stud.* **2007**, *11*, 15–29. [CrossRef]
36. Conyers, L.B. *Ground-Penetrating Radar for Archaeology*, 3rd ed.; Geophysical Methods for Archaeology; Conyers, L.B., Kvamme, K.L., Eds.; Alta Mira Press: Lanham, MD, USA, 2013; Volume 4.
37. Jervis, J.R.; Pringle, J.K.; Cassella, J.P.; Tuckwell, G. Using soil and groundwater data to understand resistivity surveys over a simulated clandestine grave. In *Criminal and Environmental Soil Forensics*; Ritz, K., Dawson, L., Miller, D., Eds.; Springer: Berlin/Heidelberg, Germany, 2009; pp. 271–284.
38. Nero, C.; Aning, A.A.; Danuor, S.K.; Noye, R.M. Delineation of graves using electrical resistivity tomography. *J. Appl. Geophys.* **2016**, *126*, 138–147. [CrossRef]
39. Carey, A.M.; Paige, G.B.; Carr, B.J.; Dogan, M. Forward modeling to investigate inversion artifacts resulting from time-lapse electrical resistivity tomography during rainfall simulations. *J. Appl. Geophys.* **2017**, *145*, 39–49. [CrossRef]
40. Frohlich, R.K.; Parke, C.D. The electrical resistivity of the vadose zone—Field survey. *Groundwater* **1989**, *27*, 524–530. [CrossRef]
41. Archie, G.E. The electrical resistivity log as an aid in determining some reservoir characteristics. *Trans. AIME* **1942**, *146*, 54–62. [CrossRef]

42. Molina, C.M.; Wisniewski, K.; Heaton, V.; Pringle, J.K.; Avila, E.F.; Herrera, L.A.; Guerrero, J.; Saumett, M.; Echeverry, R.; Duarte, M. Monitoring of simulated clandestine graves of dismembered victims using UAVs, electrical tomography, and GPR over one year to aid investigations of human rights violations in Colombia, South America. *J. Forensic Sci.* **2022**, *67*, 1060–1071. [CrossRef]
43. Barone, P.M.; Matsentidi, D.; Mollard, A.; Kulengowska, N.; Mistry, M. Mapping Decomposition: A Preliminary Study of Non-Destructive Detection of Simulated body Fluids in the Shallow Subsurface. *Forensic Sci.* **2022**, *2*, 620–634. [CrossRef]
44. Molina, C.M.; Wisniewski, K.D.; Drake, J.; Baena, A.; Guatame, A.; Pringle, J.K. Testing Application of Geographical Information Systems, Forensic Geomorphology and Electrical Resistivity Tomography to Investigate Clandestine Grave Sites in Colombia, South America. *J. Forensic Sci.* **2020**, *65*, 266–273. [CrossRef] [PubMed]
45. Abate, D.; Colls, C.S.; Moyssi, N.; Karsili, D.; Faka, M.; Anilir, A.; Manolis, S. Optimizing search strategies in mass grave location through the combination of digital technologies. *Forensic Sci. Int. Synerg.* **2019**, *1*, 95–107. [CrossRef] [PubMed]
46. Dearing, J. *Environmental Magnetic Susceptibility: Using the Bartington MS2 System*; British Library Cataloguing: London, UK, 1999.